# The Effect on Climate of Doubling Deserts

Paul A. Dirmeyer

J. Shukla

*Center for Ocean-Land-Atmosphere Studies*
*4041 Powder Mill Road, Suite 302, Calverton, Maryland 20705-3106 USA*

June 1994

## Abstract

An atmospheric general circulation model with realistic land surface properties is used to investigate the climatic effect of doubling the extent of the earth's deserts. Control and anomaly integrations are performed for 10 years. In the anomaly case, deserts are expanded over North Africa, South Africa, Australia, south-central Asia, southwestern North America, and parts of South America.

In the anomaly case, the troposphere is cooler across most of the tropics and subtropics, including all areas where desertification occurs. Annual mean precipitation is reduced over North and South Africa, south-central Asia, and Australia. Precipitation over the eastern Sahel is reduced by over 60%, and droughts persist in all seasons over northern and southern Africa. Asia and Australia exhibit weaker monsoons, but there is little effect during winter. Precipitation increases over central Africa between the two desertified regions, over the ocean equatorward of Asia and Australia during those regions' monsoons, and over the desertified areas of western North America. Regions of increased rainfall occur over the ocean to the west of the desert regions of North and South America, Australia, and South Africa. Remote effects in the winter circulation include a pronounced trough over northern Europe, and increased geopotential heights over the southern oceans.

## 1. Introduction

Charney (1975) was among the first to investigate the potential effect on climate of changes in vegetation cover in desert margins. He concluded that changes in net surface albedo directly affect the surface energy balance. In semi-arid regions, an increase in albedo leads to a loss of radiative energy from the surface, and convective overturning is reduced (Charney et al., 1977; Chervin, 1979). As a result, precipitation decreases. The ensuing reduction in vegetation cover could further enhance the albedo increase, establishing a positive feedback (Dickinson and Hanson, 1984).

Changes in surface roughness affect the balance of momentum at the surface, and can affect the efficiency of the transport of heat and moisture between land and air. Studies of reductions of roughness length over desert show that precipitation decreases unless moisture convergence is already small (Sud and Smith, 1985a). Over other land areas, reductions in roughness change rainfall patterns unsystematically, by altering the distribution of low-level convergence (Sud and Smith, 1985b; Sud et al, 1988).

Soil moisture interacts with the atmosphere via evapotranspiration, affecting the surface moisture and energy balances. Soil moisture has been found to have a positive correlation on precipitation in semi-arid regions (Namias, 1959; 1960). Modeling studies generally confirm the positive correlation between evapotranspiration and rainfall (Rind, 1982; Shukla and Mintz, 1982; Mintz, 1984; Oglesby and Erickson, 1989). However, Sud and Fennessy (1984) found precipitation to increase over arid regions when evaporation was decreased.

Changes in the biosphere affect all three of these properties. Vegetation controls transpiration and thus the transport of moisture from soil to atmosphere. The presence and

density of foliage alters radiation and momentum transfer (Dickinson, 1983). Plant canopies act to insulate the ground, mediating temperature at the surface, partially decoupling the soil from the free atmosphere (Schwartz and Karl, 1990).

There is a great deal of observational evidence that desertification has been occurring over much of the world for the last several decades. Skoupy (1987) documents the degradation of vegetation in sub-Sahara Africa over the last half-century. Pittock (1983) and Allan and Haylock (1993) describe the decrease in rainfall observed over parts of Australia since the 1940s. Dregne (1983) reports on the type and degree of desertification on each continent. Table 1 shows the percentage of land in Africa, Asia, Australia, North and South America which he defines as arid (encompassing both arid and semi-arid steppe vegetation), and the percentage of those lands which have suffered desertification due to various factors. Intensification of deserts is seen to be extensive on all of the continents examined: about half of the arid lands, principally the marginal semi-arid regions, have experienced at least moderate desertification. More recent estimates suggest 70% of drylands are affected by desertification, including 73% of rangeland and 47% of marginal farmland (Halpern,1993), affecting about one sixth of the world's population.

GCM studies have examined these effects in various regions of the world. The effects of prolonged drought and desertification on the Sahel region of Africa have been modeled extensively. One of the first studies was by Charney et al. (1977), who examined the effect of albedo increase and extremes in evaporation. Sud and Fennessy (1982; 1984) examined the effects of albedo increase and reduced evaporation separately over northern

Africa. Laval and Picon (1986) concentrated on the Sahel, where they increased albedo. Xue and Shukla (1993) changed vegetation types in a biosphere model to simulate the entire range of physical changes that accompany desertification. These studies all found precipitation to decrease as a result of simulated desertification. Sud and Molod (1988) concentrated on the effect of revegetating North Africa by decreasing surface albedo and increasing soil moisture. Xue and Shukla (1994) have likewise examined afforestation in the Sahel using a more sophisticated biosphere model.

Modeling studies have been performed for other parts of the world. Charney et al. (1977) and Sud and Fennessy (1982; 1984) also examined albedo and evaporation effects over semi-arid regions of India, North America, and the Nordeste of Brazil. The effects of albedo increase on the Asian monsoon have been studied by Meehl (1994). These studies concur that land changes analogous to desertification lead to local prolonged drought conditions.

This study is unique in that we use a sophisticated biosphere model at the lower boundary. Rather than simply altering single parameters such as albedo or roughness length, we change the distribution of vegetation types to represent expansion of desert as in Xue and Shukla (1993). However, in this study changes are made on five continents, not just over the Sahel. We attempt to represent the hypothetical global expansion of deserts by doubling the extent of deserts by intrusion into the marginal semi-arid regions. In addition, we examine the global as well as regional climate changes that widespread desertification may produce.

There are several potential causes of desertification. Expansion of deserts may be due to poor land management and destructive land use practices (Dregne, 1983; Skoupy, 1987). Desertification may be caused by the warming and drying of continents predicted by some to accompany the increase of $CO_2$ in the atmosphere (Manabe et al., 1981; 1992; Washington and Meehl, 1984; Bolin et al., 1986). On the other hand, expansion of deserts may be part of the natural variability of the climate system (Nicholson, 1979), with possible links to variations in sea surface temperature (Lamb and Peppler, 1992). It is quite possible that all three of these aspects play a role in the observed increase in desert area. We do not attempt to address the potential causes of desertification in this study. We merely attempt to ascertain the changes in climate that are likely to result from these widespread changes of the land surface.

Section 2 describes the atmospheric general circulation model (GCM), the biosphere model, and the design of the experiment. A description of the control case climatology is given in Section 3. Section 4 contains descriptions of the large-scale anomalies, while the particular effects of desertification in different regions are illustrated in Section 5. Conclusions are presented in Section 6.

## 2. Description of Experiment

Control and doubled-desert experiments are conducted using the Center for Ocean-Land-Atmosphere Studies (COLA) atmospheric general circulation model with specified lower boundary conditions over ocean and a biosphere model over land. The atmospheric GCM used is a research version of the National Meteorological Center (NMC) global

spectral model described by Sela (1980) with modifications and boundary conditions as described by Kinter et al. (1988). The model is spectral, with rhomoidal truncation at wave number 15 (R15), and is discretized into 18 vertical layers with resolution concentrated near the lower boundary. Sub-grid scale physical paramterizations are computed on a Gaussian grid with a resolution of approximately 7.5° longitude by 4.5° latitude. Complete annual and diurnal solar variations are included. Schneider and Kinter (1994) describe the current version of the model, as well as its climatology when integrated at this horizontal resolution.

The lower boundary conditions for the GCM over land are supplied by the simplified version of the Simple Biosphere (SiB) model of Sellers et al. (1986) which is described by Xue et al. (1991), and referred to hereafter as SSiB. Initial ground temperature and soil moisture are computed using the soil temperature method of Delsol et al. (1971), and the soil moisture data of Willmott et al. (1985). Over ocean, the integrations use the seasonally varying climatological sea surface temperatures of the Comprehensive Ocean-Atmosphere Data Set (COADS) Slutz et al., (1985). Aspects of the model physics and SSiB pertinent to desertification studies are described in some detail by Xue and Shukla (1993).

On the Gaussian grid, the earth's surface is comprised of 1920 grid points, of which 624 are land. There are 13 different land surface types: 11 types of vegetation-covered land as well as bare soil (which comprise the 12 vegetation types of SSiB) and permanent ice. In the control case, 34 grid points are designated as bare soil, and 49 are shrubs with bare soil (arid steppe). For this experiment, we combine these two surface types under the

designation "desert". Figure 1a shows the distribution of these two surface types in the control case. In the double-desert case, the number of desert grid points increases from 83 to 160. The number of grid points with bare soil is increased from 34 to 84. Most of the additional points are taken from adjacent steppe lands. Nonetheless, the number of steppe grid points is increased to 76 by expansion into adjacent areas. As a result, the number of points of cultivated land drops from 49 to 36, shrubs with ground cover drops from 31 to 2, savannah drops from 50 to 23, grassland drops from 14 to 10, broadleaf evergreen forest drops from 33 to 31, and broadleaf deciduous forest and mixed forest each lose one grid point. Figure 1b shows the extent of the desert region in the double-desert case.

As shown in Figure 1, desert is expanded on every ice-free continent except Europe. The core deserts are expanded, and surrounding regions are incorporated into the semi-arid steppe lands. The Sahara of Africa is intensified and the Sahel is pushed southward, similar to the experiment of Xue and Shukla (1993). The deserts of southern Africa are also expanded equatorward. The central desert of Australia is converted to bare soil, and much of the remaining continent is covered by steppe. Much of the bare soil of central Asia is in fact the rocky highland of the Himalayas. Deserts are intensified over Arabia, and expanded into the Middle East, Turkey, and the former Soviet republics of Asia. Desert is also expanded eastward in China, and Mongolia. In the Western Hemisphere, the deserts of the North American Southwest are expanded in the United States and Mexico. The coastal deserts of western South America – too narrow to be resolved at R-15 resolution – are expanded, and the Nordeste of Brazil is converted to steppe.

Control and double-desert integrations are conducted for ten years each. Initial conditions are taken from NMC analysis for 0000GMT 1 December 1990. The model is first integrated for one month to allow some equilibration of the atmosphere toward the model climate. The integrations *per se* are considered to begin on 0000GMT 1 January 1991. Since the integrations are 10 years in duration, the specific state of the initial condition can be considered unimportant in determining climatological features of the experiment. There is some evidence for climate drift in the model during the first 1-2 years, particularly in soil moisture. Time series of all fields show equilibration after year two. Therefore, only the last eight years are used for statistical calculations.

## 3. Results

In this section, we first describe the climatology of the control integration and compare mean fields for the last eight years of integration to observed data. Next, we describe the global anomalies in the double-desert integration. Finally, we concentrate on the anomalies in the desertified regions, and the systematic changes which appear to be a function of monsoon regime.

### *a. Control Integration*

Even at this relatively low resolution, the GCM produces a very good climatology. Figure 2 shows the annual mean distribution of atmospheric mass, expressed as sea level pressure (SLP), from the control integration and ECMWF analyses for the period 1980-1992. Although the zonal mean sea level pressure in the tropics is slightly high compared

to observations, the GCM simulates the tropical trough, including the low-pressure centers over the Amazon, central Africa, India, and the western Pacific. The breaks in the trough over the tropical Atlantic and East Africa are also well simulated. The oceanic high-pressure centers in the subtropics are represented in both hemispheres, as is the Tibetan anticyclone. Pressure patterns in the mid-latitudes are well depicted, especially in the Northern Hemisphere.

Figure 3 shows the annual mean 200 mb flow for the control integration and ECMWF analyses. The circulation in the tropics is very well represented from the central Pacific westward to the east coast of Africa. The GCM produces excessive westerlies over the Atlantic, and underrepresents the easterly outflow from the Amazon basin. In the extratropics, the positions of the jet cores are well simulated in the Northern Hemisphere. However, the Southern Hemisphere jet is too narrow, and the jet cores in both hemispheres are too zonal and too strong. These errors are symptomatic of the deficiency in transient kinetic energy common to all GCMs.

Annual mean precipitation from the control integration is compared to a composite of observed precipitation based on in situ and satellite measurements in Figure 4. The observed composite is prepared from 13 years (1979-1991) of satellite derived estimates over ocean of Spencer (1993), 15 years (1979-1993) from the Climate Anomaly Monitoring System (CAMS) station precipitation data archive (Ropelewski et al, 1985) gridded over land, and seven years (1986-1992) of GOES precipitation index (GPI) estimates over the tropics (Janowiak and Arkin, 1991). The Spencer data is used exclusively over the extratropical oceans, but GPI and Spencer data are averaged over oceans between 30°S and

30°N. GPI estimates are also used to fill gaps in the CAMS data over land in the tropics, and around coastlines where gaps exist due to the differing grids of the CAMS and Spencer data. No smoothing has been performed, so discontinuities may exist where different data sets abut.

The arid regions correlate well, except over the highlands of central Asia where the GCM is too wet. There is also good correspondence of rain bands in the tropics as well as the mid-latitudes. The model misses the precipitation maximum over the Bay of Bengal and Bangladesh. Also, maximum rainfall rates in the ITCZ and SPCZ are undersimulated. This is probably due to the inability of this low resolution model to accurately concentrate the ITCZ. Nonetheless, the model does a good job of capturing the major climatological precipitation features.

By comparing Figures 1 and 4, one can see that regions of bare soil in the double-desert integration largely correspond to the land areas with precipitation of less than 1 mm $d^{-1}$ in the composited data, and substantial potential evaporation. Steppes cover adjacent areas generally corresponding to areas with rainfall rates less than 2 mm $d^{-1}$. Thus, our choice of regions for expanded desert do not appear unreasonable, assuming that existing vegetation is marginal and could be easily stressed by human activity or climate fluctuations.

The model simulation of the annual cycle of precipitation over central Africa is compared to the CAMS climatologies in Figure 5. Rainfall rates are averaged between 12°E and 42°E, and plotted as a function of latitude and time. Both the CAMS and GCM mean annual cycles are computed from monthly averages. Both series show a very similar

phase and meridional range of the ITCZ, and propensity for precipitation over the Southern Hemisphere subtropics compared to similar latitudes in the Northern Hemisphere. The control integration even appears to capture the April-May maximum evident in the CAMS data, although in the model it occurs earlier and to the north. Thus, the GCM seems to simulate the oscillation between wet and dry seasons over central Africa quite well.

Figure 6 shows the corresponding time-latitude plot for the monsoon region of Asia (65°E-105°E). Here the model underestimates both the strength of the monsoon precipitation, and the northward traverse of the monsoon. There is also a tendency in the GCM for the ITCZ over the Indian Ocean to remain in the Northern Hemisphere throughout the year, although in individual years the ITCZ sometimes moves south of the equator (not shown). This further mutes the contrast between wet and dry seasons in this region. Spatial resolution in the model may again play a role. The structure of the Tibet plateau, especially the steep southern face, is poorly resolved at R-15, and the massif of the Indian subcontinent is practically unresolved. Nevertheless, the region between 12°N and 23°N in the control integration receives at least 60% of its annual rainfall during May-October.

## 4. Large-Scale Anomalies

In this section we focus on the climate anomalies (double-desert minus control) with particular concentration on the principal large-scale features. Anomaly patterns over specific regions will be discussed in the next section.

*a. Low-Latitude Cooling*

The net surface albedo of the bare soil regions is higher than the net albedo of the other vegetation types. The steppe vegetation has the second highest net albedo. Thus, the desertified areas can be expected to absorb less solar radiation than in the control case. One consequence of an increase in albedo and a decrease in absorbed radiation is a concomitant cooling of the troposphere over those areas (Charney et al., 1977). This is indeed the case in this experiment, although the cooling is not confined to the immediate areas of desertification. Figure 7a shows the anomaly of 850-200 hPa thickness. The largest negative anomalies are found over southwestern Asia, North Africa and the subtropical North Atlantic. However, the region of significant (95%) negative temperature anomalies covers much of the tropics and subtropics. A contiguous area extends from the central tropical Pacific across Central America and most of South America, the Caribbean Sea, the entire tropical and subtropical Atlantic, all of Africa, most of Europe, a wide zonal band of Asia from the Mideast to Korea, and a similar zonal band in the Southern Hemisphere from South Africa to southern Australia. This region encompasses most of the desert areas, but also covers additional territory nearly three times the area of all expanded deserts. There are only small regions of significant positive anomalies over the northeastern U.S. and the North Pacific. Positive surface pressure anomalies exist over most of the desertified regions, with a broad area of small but significant negative anomalies over most of the tropics and subtropics from the Indian ocean eastward to the eastern Pacific (not shown).

The major contribution to this cooling anomaly in the annual mean comes during the boreal summer. During this period, negative temperature anomalies in the mid-troposphere exceed 1.5 K over northwestern Africa as well as Kurdistan (not shown). In addition to the significant Northern Hemisphere anomalies, there is also significant cooling over southern Africa and the subtropical South Atlantic. During southern summer, significant cooling anomalies are largely confined to the Southern Hemisphere with the exception of West Africa and the subtropical North Atlantic, where negative anomalies of 0.6 K persist in the mid-troposphere.

The surface temperature decreases over most of the desertified regions, although increases do occur in some areas, particularly during summer and where cloud cover is significantly reduced (Figure 7b). Meanwhile, there is an increase in net longwave radiation upward from the surface in most of the areas. However, there is less heating of the atmosphere because of the combination of reduced surface latent heat flux due to removal of vegetation, and decreased sensible heat flux owing to reduced surface roughness. The net effect over the expanded deserts is a cooling of the troposphere. The atmospheric circulation disperses the cooler air, spreading it westward in the tropics, and eastward in the subtropics and mid-latitude margins. Some of the increase in net longwave radiation is due to the contrast between cooler troposphere in the temperature and the generally warmer surface.

*b. Precipitation*

Anomalies for annual mean precipitation and their statistical significance are shown in Figure 8a. The largest negative anomalies occur over the Sahel of northern Africa. There are also significant negative anomalies over the desertified regions of southern Africa. It is interesting to note that not all desertified areas show significant decreases in precipitation. In fact, there is a region of significant increase in rainfall over southwestern North America. Also, there are regions which experience significant drops in precipitation where vegetation was not altered, most notably over southern Asia. A significant shortfall exists over the northern Bay of Bengal, Myanmar, and a large part of China. Negative anomalies also appear over much of the North Atlantic, and scattered smaller areas.

Accompanying the regions of decreased precipitation are areas of significant positive anomalies in the annual mean. Equatorial Africa between the two deserts shows the greatest increase. This region of positive anomalies extends westward across the Atlantic, and then northwest along the coast of South America to the subtropical western North Atlantic. This north-south dipole is similar to that simulated by Xue and Shukla (1993) for Sahel desertification. There are also positive anomalies over ocean to the west of the deserts of South Africa, Australia, and western South America. The positive anomalies extend around the oceanic poleward sides of South Africa and Australia, similar to the anomalies in the idealized subtropical desertification study of Dirmeyer (1992).

Figure 8b shows the precipitation anomalies expressed as a percentage of annual mean rainfall. It shows that the greatest impact of the negative anomalies in northern Africa are to the north of the band of highest magnitude. Rainfall decreases by more than

60% over Sudan. Almost the entire area of North Africa and the Mideast experience at least a 20% decrease, as does much of South Africa. Shortfalls over Australia and monsoonal Asia are generally 10%. Much of western tropical Africa experiences a 10-40% increase in rainfall. There are also 10-20% increases over the desertified region of southwestern North America, and the oceanic positive anomaly centers to the west of the Southern Hemisphere deserts.

*c. Extratropical Anomalies*

Geopotential height anomalies at 200 hPa are shown in Figure 9 for boreal winter (DJF) and austral winter (JJA). The broad areas of negative anomalies at low-latitudes reflect the tropospheric cooling described previously. There are also significant anomalies in the extratropics, particularly during austral winter. However, we will first focus on DJF (Figure 9a). There is a significant negative height anomaly centered over the Baltic region. The maximum anomaly is 52 m, and much of Europe is covered by a significant decrease in geopotential height. This area is associated with a negative tropospheric temperature anomaly, and an increase in interannual variability over western Russia during the same season (not shown). There is an equally strong positive height anomaly over the North Atlantic, but only a very small area south of Nova Scotia is statistically significant. A weak negative anomaly also exists over northwestern Canada. In the summer hemisphere, a negative anomaly comparable to the one over the Baltic Sea exists to the east of New Zealand.

During JJA (Figure 9b), the high-latitudes of the Southern Hemisphere are covered by positive height anomalies, with significant deviations along much of the Antarctic coast and adjacent oceans. The Antarctic anomalies appear to be part of a meridional redistribution of mass to compensate for the falling surface pressures in the tropics. Anomalies in surface pressure (not shown) show significant increases over the southern oceans during JJA, with smaller increases in other seasons. It is interesting to note that height anomalies similar to DJF exist over the high-latitudes of the Northern Hemisphere. Although the magnitude of these summer anomalies is less then their winter counterparts, the regions of statistical significance cover about the same area. In fact, there is a significant decrease in the interannual variability of surface pressure over the North Atlantic. The robust nature of these features suggest they may be part of an anomalous stationary wave pattern forced from the large desertified region in North Africa. North Africa is the likely origin due to its proximity and the dominant strength of the heating anomalies there.

**5. Monsoon Circulations**

Examination of the precipitation anomalies indicates there are three categories of response to desertification. First, there are the regions which experience year round negative anomalies in precipitation. Both northern and southern Africa fit into this category. Second, there are regions which experience significant decreases in precipitation only during the summer. The "true" monsoon areas of southern Asia and Australia are in this category (by "true" we mean monsoon circulations driven by land-sea contrast, and not

the migration of a land-locked ITCZ between hemispheres as occurs in the "land" monsoons of Africa). Finally, there are the areas exhibiting little or no systematic shortfalls of precipitation during any season. These include the desertified regions of the Western Hemisphere.

*a. Africa*

The semi-arid regions of both northern and southern Africa where desert was expanded are regions of strong seasonality in rainfall. These regions experience a distinct rainy season during summer, and a dry season during winter (Nicholson, 1986). These seasons are a manifestation of the differential heating of land between the two hemispheres, and the migration of the ITCZ north and south over land. Western Africa differs somewhat in that there is a meridional land-sea contrast rather than a warm land-cool land contrast, but the coastal region is close enough to the equator that the ITCZ migrates over land in that area as well (Meehl, 1992).

Figure 10 shows the mean annual cycle of the surface moisture balances for the control case and the anomaly (double-desert minus control) for the desertified regions of northern and southern Africa. The annual cycle is averaged over only those areas where vegetation has been changed between experiments. The area for North Africa includes desertified points within the box 20°W-49°E, 0°N-50°N (see Figure 1). The desertified regions of western Asia which are outside the Asian monsoon regime are included with North Africa. Areas of Africa south of the equator are averaged in Figures 10c, d. There are clear wet and dry seasons in each region (Figures 10a, c), with variations in mean

monthly rainfall of nearly an order of magnitude in both north and south. The rainy and dry periods are synonymous with periods of high and low evapotranspiration respectively. Soil moisture is seen to recharge during the onset of the wet season, and deplete during the dry season. Runoff is highest after the initiation of the wet season.

Desertification in Africa is found to cause negative anomalies in precipitation during both wet and dry seasons (Figures 10b, d). Although the magnitudes of the anomalies are much smaller during the dry season, the percentage decrease in rainfall is not a strong function of season. In the north, the minimum reduction in monthly rainfall expressed as a percentage is 25% in November, with the largest decrease being nearly 50% in March. Reductions in the south vary between 5-40%. Although the mean values of precipitation and evapotranspiration vary in a similar fashion throughout the year, the evapotranspiration anomaly has a much smaller annual swing than the precipitation anomaly. The same is true of runoff and change in soil moisture. The effect of the consistent decrease in evapotranspiration is to decrease the annual variation of P-E. Thus, atmospheric moisture flux convergence decreases during the rainy season, and the export of moisture through flux divergence during the dry season is reduced. This means that over Africa, there is a reduction in the amount of cross-equatorial moisture advection from the winter to the summer hemisphere. The ITCZ rainband does not suffer, however. As shown in Figure 8, rainfall in the African ITCZ increases. Figure 11 shows the annual cycle of precipitation over Africa averaged between 12°E-42°E in the double-desert case, and the anomaly. There is actually a narrowing of the range of the ITCZ, accompanied by intensification and a slight shift southward. Rainfall decreases on the poleward margins of the ITCZ in the

summer hemisphere. This occurs despite the fact that surface temperatures in the summer hemisphere subtropics are 1-2 K warmer, and winter surface temperatures 1-2 K cooler in the double-desert case. The equatorward margin of the desertified region of northern Africa maintains positive anomalies of 0.5-1 K in winter and summer. The reduced low-level convergence over the desertified areas leaves more moisture available in the tropics, and more precipitation can occur. However, the equatorward intrusion of desert confines the ITCZ to a narrower region.

Figure 12 shows the annual cycle of terms in the surface energy balance for the control case and anomalies over northern and southern Africa, defined as in Figure 10. The solar driving force of the differential heating is evident in the cycle of absorbed shortwave radiation. Weaker cycles of sensible and latent heat flux are evident in the control cases (Figures 12a, c). The increase of albedo in the desertified areas leads to negative anomalies in absorbed shortwave radiation (Figures 12b, d). The decrease is accompanied by a reduction in sensible heat flux in both areas. The reduction in evapotranspiration seen in Figure 10 is represented by the negative anomaly in latent heat flux. The negative latent heat flux anomaly matches the anomalies in sensible heat flux and absorbed shortwave radiation during the dry season, and exceeds them during the wet season. Surface temperature increases because the reductions in surface fluxes outpace the reduction in absorbed solar radiation, particularly in summer. As a result, there is an increase in net longwave radiation escaping the surface. Also, the anomalies in latent heat flux and net longwave radiation reduce the magnitude of the annual cycle in these terms.

Along with reduced annual variability, there is also a reduction in the interannual variability of many climate variables over Africa. Precipitation, precipitable water, and most surface energy terms show a significant reduction in interannual variability over the Sahel. However, surface latent and sensible heat flux variability increase over equatorial Africa. There is also an increase in the variability of the upper-troposphere winds over central Africa and the Sahel. These changes accompany a strong westerly anomaly in winds over the western part of the region (not shown) which strongly retard the Somali jet.

*b. Asia and Australia*

Both southern Asia and Australia are situated such that they lay predominantly in the subtropics adjacent to equatorial oceans. These areas experience well defined monsoons, driven by the seasonal oscillation of contrasts between the heating of land and sea. Thus, the annual cycle over these regions differs from that of the land-land cycle over Africa. The monsoons of southern Asia are intensified by the elevated heat source of the Tibetan plateau to the north (Murakami, 1987; Yanai and Li, 1994). The Australian monsoon may be somewhat weakened by the presence of the many islands of Indonesia, which act as numerous small heat sources for the atmosphere and help anchor the center of low-level convergence near the equator (Meehl, 1992). Nonetheless, in determining the response of climate to desertification, the differences between Australia and Asia appear to be less important than their shared differences from Africa.

Figure 13 shows the surface moisture balances for southern Asia and Australia. Again, only land points where vegetation has been changed are included in the calculation,

over 60°E-120°E, 5°N-40°N for Asia, and 100°E-160°E, 10°S-40°S for Australia (see Figure 1). Both areas show strong seasonality with precipitation and evapotranspiration in phase, like Africa. Australia shows little variation in soil moisture or runoff. Both regions are also similar to Africa in having large negative rainfall anomalies during summer. However, neither Asia nor Australia have appreciable negative anomalies during the dry season. In fact, both regions show small to moderate positive rainfall anomalies in some months.

Another critical difference is the relatively small and seasonal evapotranspiration anomalies over Asia/Australia compared to Africa. Although negative anomalies exist over Asia in all months, they do not exceed 10% in any month. This is in contrast to the 25-50% shortfalls over Africa. In Australia, evapotranspiration anomalies are negligible throughout the dry season, and are actually positive during September and October. Negative anomalies do approach 25% at the onset of the wet season but are otherwise small. One might assume that since these are areas where deserts have been intensified more than they have been expanded, that evapotranspiration was already limited in the control case, and there is little room for change. However, control case evapotranspiration rates over Africa (particularly northern Africa) are as low or lower than over Asia and Australia, yet Africa experiences a sharp decrease in evapotranspiration. We do not believe vegetation contrasts are the sole factor in determining the differing responses; land-sea geometry and orography also play a role.

Figure 14 shows the annual cycle of rainfall in the double-desert case averaged over monsoonal Asia (65°E-105°E), as well as the anomalies. There is a decrease in rainfall

along the entire leading edge of the monsoon. Rainfall in the south is reduced during April and May. The deficit migrates north during the peak of the monsoon, while rainfall over extreme southern India, Sri Lanka, Malaysia and the Indian Ocean increases. Deficits spread south again with the receding monsoon during fall.

The weak response in latent heat flux to desertification is clear in the annual cycle of the surface energy balance over Asia and Australia (Figure 15). As over Africa, decreases in absorbed shortwave radiation are matched closely by reductions in sensible heat flux. But there is little change in latent heat flux, especially during the dry season, so net longwave radiation is not affected. An exception is during the wet season over Australia, where the increase in longwave flux resembles the patterns in Africa. Australia has a more complicated pattern of surface temperature anomalies than Africa (not shown). There is generally an increase in surface temperature over central Australia, with cooling along the coasts. This pattern is present to some degree in all seasons. Most of monsoonal Asia is slightly warmer during summer and cooler during winter, except for southwestern Asia for which the opposite pattern occurs.

*c. Other Regions*

The desertified regions of the Americas have a different geometry than those of the Eastern Hemisphere. Whereas the deserts of Africa, Asia and Australia lie predominantly in zonal bands, the mountain ranges of the Andes and Rockies constrain the zonal extent of the American deserts. Also, there is little land in the subtropics. The continents are narrow at Mexico and the Pampas: they are wide in the tropics at the Amazon Basin and

in the mid-latitudes of the United States and Canada. Consequently, there are no comparably balanced areas of land in the subtropics and tropics as in Africa, nor are there clear meridional delineations between subtropical land and tropical ocean as with Asia and Australia. This geometry limits both the area of strong seasonality of precipitation, and the intensity of the seasonality. The margins of the Amazon Basin exhibit wet-dry oscillations similar to Africa (Nobre et al., 1991), but the Andes divide the eastern subtropical lands, characterized by strong maritime influence and dependable rain, from the severe deserts of the west coast. The Nordeste is a semi-arid tropical region with an unique climate strongly dependent on conditions in the tropical Atlantic (Moura and Shukla, 1981; Hastenrath and Greischar, 1993). Extreme southwestern North America has a weak summer monsoon circulation (Bryson and Lowery, 1955; Douglas et al., 1993), but nothing as dramatic and dependable as in Asia or northern Australia.

The desert regions of southwestern North America, western South America, and the Nordeste region of Brazil have been examined separately. Desertified points as indicated in Figure 1 are included for each region. Figure 16 shows the annual cycle of the moisture balance in these three areas. There is not a dominant summer rainy season in any of these areas. Also, none of these areas exhibit the strong phase-locking of evapotranspiration to precipitation that was evident in the other regions. The Nordeste shows a weak tendency for phase-locking, but evapotranspiration does not reflect the heavy precipitation of March-May.

We find that in the doubled-desert case, there is little drought signal in the Americas. The anomaly plots (Figures 16b, d, f) show sporadic precipitation anomalies

in each area. The desert region of North America has positive rainfall anomalies in most months, with increased runoff but little change in evapotranspiration. Western South America shows a persistent negative anomaly during the summer, although there is no specific rainy season at that time. This anomaly is largely confined to the northern extreme of the desertified area — most of the region has no significant anomaly. Large monthly anomalies exist over the Nordeste, but there is little pattern. If anything, there seems to be a semi-annual signal, with negative anomalies in the wet and dry seasons, and positive anomalies during the transitions. Recall from Figure 8 that while there is a weak negative rainfall anomaly over the region, there are significant positive anomalies just off the coast. These centers, which are fairly robust across seasons, may be contributing to the intermittent positive anomalies. Much longer integrations would be necessary to establish significance in these weak patterns.

## 6. Summary and Conclusions

In this study, we have examined the effect on climate of doubling the extent of the world's deserts by use of a GCM with a realistic representation of fluxes between the atmosphere and land surface/biosphere (SSiB). The double-desert case represents an extreme scenario of desertification which might ensue as a result of combined natural and anthropogenic causes. Desert-type vegetation is intensified and expanded in five regions: North Africa, South Africa, southern Asia, Australia and southwestern North America. Desert is also introduced in western South America (where its current extent is too zonally small to be resolved by the GCM), and the Nordeste region of Brazil.

We have found that the doubling of desert area results in significant cooling over much of the tropics and subtropics. The anomalously cool air is not limited to only the desert regions, but is dispersed by the atmospheric circulation to cover an area nearly six times the size of the current deserts as represented by SSiB. This cooling weakens slightly the temperature contrast between the equator and the poles in the troposphere. Global mean air temperature drops 0.2 K at 700 hPa, and negative anomalies of at least 0.1 K occur from 900-250 hPa.

Another effect of expanding deserts is a change in the distribution of precipitation. Rainfall generally, but not invariably, decreases over desertified areas. Over Africa the decreases are large. Moderate decreases occur over southeast Asia and Australia. Precipitation increases over southwestern North America. There are also increases over equatorial Africa, the tropical Atlantic and Indian oceans, and over ocean to the west and southwest of the desertified areas of the Southern Hemisphere.

There are significant anomalies in the extratropical circulation as well. Tropospheric temperatures over Europe are cooler, and an anomalous trough persists over northern Europe throughout the year. A ridge of large comparable magnitude but marginal significance is situated over the North Atlantic. There are significant positive height anomalies over the high-latitudes of the Southern Hemisphere during southern winter.

Areas of desertification experience an increase in net surface albedo, and decreased surface roughness. These changes combine to reduce the flux of energy from the surface by decreasing the percentage of solar radiation absorbed, and limiting the mechanical transport of thermal energy away from the surface by sensible heating. Transpiration is

also reduced by the removal of vegetation, so latent heat flux is also curtailed. The reduction in heat flux from the surface leads to a cooling of the atmosphere. Depending on the relative strengths of the reductions in absorbed solar radiation and heat flux, the surface temperature may rise or fall. Both situations occur in the double-desert case. Some areas are consistently warmer or cooler, while others experience an increase in the annual cycle of surface temperature: warmer in summer and cooler in winter. Regardless, cloud cover generally decreases, allowing more longwave radiation from the surface to escape into space, further cooling the troposphere.

Decreased surface heating over the intensified deserts of the subtropics can also lead to increased local subsidence by another means. The presence of cooler mid-troposphere air over adjacent oceans and land unaffected by desertification, described previously, decreases the static stability of the atmosphere in those areas. Meanwhile, moist static energy decreases over the desertified regions. The contrast in moist static energy between the deserts and surrounding areas is enhanced, making the surrounding areas even more favorable for moist convection. Such a rise in convection over adjacent areas reinforces the overturning circulation and, by continuity, augments subsidence over the desert regions, further depriving them of moisture and rainfall. This mechanism does not appear to act uniformly over all desertified regions.

Africa appears to suffer the greatest impact in this study. Precipitation is reduced by more than 50% over much of the Sahel. In both northern and southern Africa, the negative precipitation anomalies are a year-round feature. The magnitudes of the anomalies vary in accordance with the rainy and dry seasons, but the percentage reductions in rainfall

are rather stable throughout the year. Between the dry, desertified areas is a region of increased rainfall over tropical Africa where the surface was not changed. The ITCZ appears to narrow and intensify, while crossing a smaller meridional range with the seasons. The intensified low-level convergence over equatorial Africa is fed by moisture from both the winter and summer hemispheres.

Asia and Australia, like Africa, experience pronounced drought during the summer rainy season. The mechanism is similar, although it appears to be the reduced contrast in heating between desert land and ocean, rather than desert land versus vegetated land, that perpetuates the drought. Like over Africa, an enhancement of tropical rainfall equatorward of these areas accompanies the summer droughts. However, since winter heating of the land is minimal regardless of the vegetation, and since Asia and Australia are not flanked by corresponding desertified land areas on the opposite side of the equator, there is no mechanism to enhance tropical low-level convergence during local winter so precipitation does not decrease during the dry season. Also, Asia and Australia are somewhat more influenced by mid-latitude storms during winter than the southern flank of the Sahara or South Africa. Precipitation driven by baroclinic instability is relatively insensitive to changes in vegetation.

The desert regions in the Americas have the weakest response. These areas are somewhat smaller, and have a more meridional than zonal orientation. Consequently, they do not impact the regional Hadley circulation as strongly as the other regions. The regions in western North and South America have weak, localized monsoons which are not evident when the entire area of desertification is taken into account. These areas are also montane,

and extend into mid-latitudes where the abundance of baroclinic weather systems reduces the importance of vegetation change on climate. The Nordeste region of Brazil is the smallest of the desertified regions in this study. There is some indication of a decrease in precipitation during the wet season, but the anomalies are sporadic in sign and magnitude throughout the year, and of marginal significance. The Nordeste also appears to be on the edge of the region of increased precipitation induced by the changes in North Africa and their effect on the Hadley and Walker circulations. Thus, the local response may be masked by the remote response due to more widespread changes elsewhere.

## References


Allan, R. J., and M. R. Haylock, 1993: Circulation features associated with the winter rainfall decrease in southwestern Australia. *J. Climate,* **6,** 1356-1367.

Bolin, B., B. R. Döös, J. Jager, and R. A. Warrick, 1986: The Greenhouse Effect, Climate Change and Ecosystems. *Wiley and Sons,* New York, 541pp.

Bryson, R. A., and W. P. Lowery, 1955: Synoptic climatology of the Arizona summer precipitation singularity. *Bull. Amer. Meteor. Soc.,* **36,** 329-229.

Charney, J. G., 1975: Dynamics of deserts and drought in the Sahel. *Quart. J. Roy. Meteor. Soc.,* **101,** 193-202.

Charney, J. G., W. J. Quirk, S. H. Chow, and J. Kornfield, 1977: A comparative study of the effects of albedo change on drought in semi-arid regions. *J. Atmos. Sci.,* **34,** 1366-1385.

Chervin, R. M., 1979: Response of the NCAR general circulation model to changed land surface albedo. *Report of the JOC Study Conference on Climate Models: Performance, Intercomparison and Sensitivity Studies, Washington, D.C., GARP Publ. Series, No. 22,* Vol 1, 563-581.

Delsol, F., K. Miyakoda, and R. H. Clarke, 1971: Parameterized processes in the surface boundary layer of an atmospheric circulation model. *Quart. J. Roy. Meteor. Soc.,* **97,** 181-208.

Dickinson, R. E., 1983: Land surface processes and climate-surface albedos and energy balance. *Advances in Geophysics, Vol. 25,* Academic Press, 305-353.

Dickinson, R. E., and B. Hanson, 1984: Vegetation-albedo feedbacks. *Climate Processes and Climate Sensitivity, Geophysical Monograph 29, Maurice Ewing Volume 5,* American Geophysical Union, 180-186.

Dirmeyer, P. A., 1992: GCM studies of the influence of vegetation on the general circulation. *PhD Dissertation, [Available from University of Maryland, College Park, MD 20742,* U.S.A.], 227pp.

Douglas, M. W., R. A. Maddox, K. Howard, and S. Reyes, 1993: The Mexican monsoon. *J. Climate,* **6,** 1665-1677.

Dregne, H. E., 1983: Desertification of Arid Lands. *Advances in Desert and Arid Land Technology and Development, Volume 3, Harwood Academic,* New York, 242pp.

Halpern, S. L., 1993: The United Nations Conference on Environment and Development: Process and documentation. *Academic Council on the United Nations System Reports and Papers 1993 No. 2,* Providence, RI

Hastenrath, S., and L. Greischar, 1993: Further work on the prediction of Northeast Brazil rainfall anomalies. *J. Climate.,* **6,** 743-758.

Janowiak, J. E., and P. A. Arkin, 1991: Rainfall variations in the tropics during 1986-89, as estimated from cloud-top temperatures. *J. Geophys. Res.,* **96,** 3359-3373.

Kinter, J. L., J. Shukla, L. Marx and E. K. Schneider, 1988: A simulation of the winter and summer circulations with the NMC global circulation model. *J. Atmos. Sci.,* **45,** 2486-2522.

Lamb, P. J. , and R. A. Peppler, 1992: Further case studies of tropical Atlantic surface atmospheric and oceanic patterns associated with Sub-Saharan drought. *J. Climate,* **5,** 476-488.

Laval, K., and L. Picon, 1986: Effect of a change of the surface albedo of the Sahel on climate. *J. Atmos. Sci.,* **43,** 2418-2429.

Manabe, S., M. J. Spelman, and R. J. Stouffer, 1992: Transient responses of a coupled ocean-atmosphere model to gradual changes of atmospheric CO2. Part II: Seasonal response. *J. Climate,* **5,** 105-126.

Manabe, S., R. T. Wetherald, and R. J. Stouffer, 1981: Summer dryness due to an increase of atmospheric CO2 concentration.. *Clim. Change,* **3,** 347-386.

Meehl, G. A., 1992: Effect of tropical topography on global climate. *Annu. Rev. Earth Planet. Sci.,* **20,** 85-112.

Meehl, G. A., 1994: Influence of the land surface in the Asian summer monsoon: External conditions versus internal feedbacks. *J. Climate,* (in press).

Mintz, Y., 1984: The sensitivity of numerically simulated climates to land-surface boundary conditions. *The Global Climate, J. Houghton, ed.,* Cambridge University Press, 79-105.

Moura, A. D., and J. Shukla, 1981: On the dynamics of droughts in northeast Brazil: Observations, theory and numerical experiments with a general circulation model. *J. Atmos. Sci.,* **38,** 2653-2675.

Murakami, T., 1987: Orography and monsoons. *Monsoons, Eds: J. S. Fein and P. L. Stevens, Wiley and Sons,* New York, 331-364.

Namias, J., 1959: Persistence of mid-troposheric circulations between adjacent months and seasons. *The Atmosphere and the Sea in Motion, B. Bolin, ed.,* Rossby Memorial Volume, 240-248.

Namias, J., 1960: Factors in the initiation, perpetuation and termination of drought. *[Extract of publication No. 51,* I.A.S.H. Commission of Surface Waters], 81-94.

Nicholson, S. E., 1986: The spatial coherence of African rainfall anomalies; interhemispheric teleconnections. *J. Climate Appl. Meteor.,* **25,** 1365-1381.

Nicholson, S. E., 1979: Revised rainfall series for the West African subtropics. *Mon. Wea Rev.,* **107,** 620-623.

Nobre, C. A., P. J. Sellers, and J. Shukla, 1991: Amazonian deforestation and regional climate change. *J. Climate,* **4,** 957-988.

Oglesby, R. J., and D. J. Erickson III, 1989: Soil moisture and persistence of North American drought. *J. Climate,* **1,** 1362-1380.

Pittock, A. B., 1983: Recent climate change in Australia: Implications for a CO2 warmed earth. *Clim. Change,* **5,** 321-340.

Rind, D., 1982: The influence of ground moisture conditions in North America on summer climate as modeled in the GISS GCM. *Mon. Wea Rev.,* **110,** 1487-1494.

Ropelewski, C. F., J. E. Janowiak, and M. F. Halpert, 1985: The analysis and display of real time surface climate data. *Mon. Wea Rev.,* **113,** 1101-1107.

Schneider, E. K., and J. L Kinter III, 1994: An examination of internally generated variability in long climate simulations. *Climate Dyn.*, (in press).

Schwartz, M. D., and Y. R. Karl, 1990: Spring Phrenology: Nature's experiment to detect the effect of "Green-Up" on surface maximum temperatures. *Mon. Wea Rev.,* **118,** 883-890.

Sela, J. G., 1980: Spectral modeling at the National Meteorological Center. *Mon. Wea. Rev.*, **108,** 1279-1292.

Sellers, P. J., Y. Mintz, Y. C. Sud, and A. Dalcher, 1986: A simple biosphere model (SiB) for use within general circulation models. *J. Atmos. Sci.*, **43,** 505-531.

Shukla, J., and Y. Mintz, 1982: Influence of land-surface evapotranspiration on the earth's climate. *Science,* **215,** 1498-1501.

Skoupy, J., 1987: Desertification in Africa. Agricultural and meteorological programs. *Proc. Regional Training Seminar on Drought and Desertification in Africa, Addis Ababa,* World Meteorological Organization, 33-45.

Slutz, R. J., S. J. Lubker, J. D. Hiscox, S. D. Woodruff, R. L. Jenne, D. H. Joseph, P. M. Streurer, and J. D. Elms, 1985: COADS: Comprehensive Ocean-Atmosphere Data Set. Release 1. *[Available from Climate Research Program, Environmental Research Laboratories, 325 Broadway, Boulder,* CO 80303.], 262 pp.

Spencer, R. W., 1993: Global oceanic precipitation from the MSU during 1979-91 and comparisons to other climatologies. *J. Climate,* **6,** 1301-1326.

Sud, Y. C., and M. Fennessy, 1982: A study of the influence of surface albedo on July circulation in semi-arid regions using the GLAS GCM. *J. Climatol.*, **2,** 105-125.

Sud, Y. C., and M. J. Fennessy, 1984: Influence of evaporation in semi-arid regions on the July circulation: A numerical study. *J. Climatol.*, **4,** 383-398.

Sud, Y. C., and W. E. Smith, 1985: Influence of local land-surface processes on the Indian monsoon: A numerical study. *J. Climate Appl. Meteor.*, **24,** 1015-1036.

Sud, Y. C., and W. E. Smith, 1985: The influence of surface roughness of deserts on the July circulation (A numerical study). *Boundary-Layer Meteor.*, **33,** 15-49.

Sud, Y. C., J. Shukla, and Y. Mintz, 1988: Influence of land surface roughness on atmospheric circulation and precipitation: A sensitivity study witn a general circulation model. *J. Appl. Meteor.*, **27,** 1036-1054.

Washington, W. M., and G. A. Meehl, 1984: Seasonal cycle experiment on the climate sensitivity due to a doubling of CO2 with an atmospheric general circulation model coupled to a simple mixed-layer ocean model. *J. Geophys. Res.*, **89,** 9473-9503.

Willmott, C. J., C. M. Rowe, and Y. Mintz, 1985: Climatology of the terrestrial seasonal water cycle. *J. Climatol.*, **5,** 589-606.

Xue, Y., and J. Shukla, 1993: The influence of land surface properties on Sahel climate: Part I - Desertification. *J. Climate,* **6,** 2232-2245.

Xue, Y., and J. Shukla, 1994: The influence of land surface properties on Sahel climate. Part 2: Afforestation. *J. Climate,* (submitted).

Xue, Y., P. J. Sellers, J. L. Kinter and J. Shukla, 1991: A simplified biosphere model for global climate studies. *J. Climate,* **4,** 345-364.

Yanai, M., and C. Li, 1994: Mechanism of heating and the boundary layer over the Tibetan plateau. *Mon. Wea Rev.,* **122,** 305-323.

## Figures

1. Location of bare soil and steppe vegetation (shrubs with bare soil) in; (a) control case; (b) double desert case.
2. Time mean sea level pressure for; (a) last eight years of the control case; (b) 13 years of ECMWF analyses (1980-1992). Contour interval 4 hPa with the 1010 hPa contour included over the tropics.
3. Time mean winds at 200 hPa for; (a) last eight years of the control case; (b) 13 years of ECMWF analyses (1980-1992). Shading indicates wind speed in m $s^{-1}$.
4. Time mean precipitation rate for; (a) last eight years of the control case; (b) composited station and satellite-derived observations (see text for description). Shading indicates rainfall rate in mm $d^{-1}$.
5. Mean annual cycle of climatological precipitation as a function of latitude averaged between 12°E-42°E; (a) gridded CAMS station data; (b) control case. Units are mm $d^{-1}$.
6. Mean annual cycle of climatological precipitation as a function of latitude averaged between 65°E-105°E; (a) gridded CAMS station data; (b) control case. Units are mm $d^{-1}$.
7. Mean 850-200 hPa thickness anomalies (a), and surface temperature anomalies (b) for last eight years of integrations. Contour interval is 5 m in (a), 0.3 K in (b), zero contour is omitted. Shading indicates significance at 5%.

8. Mean precipitation anomalies (double desert minus control) for last eight years of integrations; (a) in mm $d^{-1}$, contour interval is 0.3; (b) as percentage of control rainfall, contour interval is 10%. Zero contours are omitted, Shading indicates significance at 5%.

9. Mean geopotential height anomalies (double desert minus control) at 200 hPa for last eight years of integrations; (a) December-February; (b) June-August. Contours at ±10, ±20, ±40, ±60 m. Shading indicates significance at 5%.

10. Time series of mean monthly surface moisture balance terms for; (a) North Africa control case; (b) North Africa anomaly (double desert minus control); (c) South Africa control case; (d) South Africa anomaly. Units are mm $d^{-1}$. Open circles: precipitation, filled circles: evapotranspiration, open squares: runoff, filled squares: change in soil moisture. Negative precipitation anomalies are shaded.

11. Mean annual cycle of double-desert precipitation (shaded) and anomaly (contours) as a function of latitude averaged between 12°E-42°E. Units are mm $d^{-1}$.

12. Time series of mean monthly surface energy balance terms for; (a) North Africa control case; (b) North Africa anomaly (double desert minus control); (c) South Africa control case; (d) South Africa anomaly. Units are W $m^{-2}$. Open circles: absorbed shortwave radiation, filled circles: net longwave radiation (upward), open squares: sensible heat flux, filled squares: latent heat flux.

13. Time series of mean monthly surface moisture balance terms for; (a) Asia control case; (b) Asia anomaly (double desert minus control); (c) Australia control case; (d) Australia anomaly. Units are mm $d^{-1}$. Open circles: precipitation, filled circles:

evapotranspiration, open squares: runoff, filled squares: change in soil moisture. Negative precipitation anomalies are shaded.

14. Mean annual cycle of double-desert precipitation (shaded) and anomaly (contours) as a function of latitude averaged between 65°E-105°E. Units are mm $d^{-1}$.

15. Time series of mean monthly surface energy balance terms for; (a) Asia control case; (b) Asia anomaly (double desert minus control); (c) Australia control case; (d) Australia anomaly. Units are W $m^{-2}$. Open circles: absorbed shortwave radiation, filled circles: net longwave radiation (upward), open squares: sensible heat flux, filled squares: latent heat flux.

16 Time series of mean monthly surface moisture balance terms for; (a) North America control case; (b) North America anomaly (double desert minus control); (c) western South America control case; (d) western South America anomaly; (e) western Nordeste control case; (f) Nordeste anomaly. Units are mm $d^{-1}$. Open circles: precipitation, filled circles: evapotranspiration, open squares: runoff, filled squares: change in soil moisture. Negative precipitation anomalies are shaded.

**Table 1** Areas of arid lands and desertification on five continents (adapted from data of Dregne, 1983).

| | | Moderate/Severe Desertification | |
|---|---|---|---|
| | % Continent that is Arid | % of Arid Land | % of Continent |
| Africa | 57% | 28% | 16% |
| Asia | 36% | 49% | 17% |
| Australia | 83% | 56% | 52% |
| North America | 18% | 90% | 16% |
| South America | 17% | 56% | 10% |

Figure 1

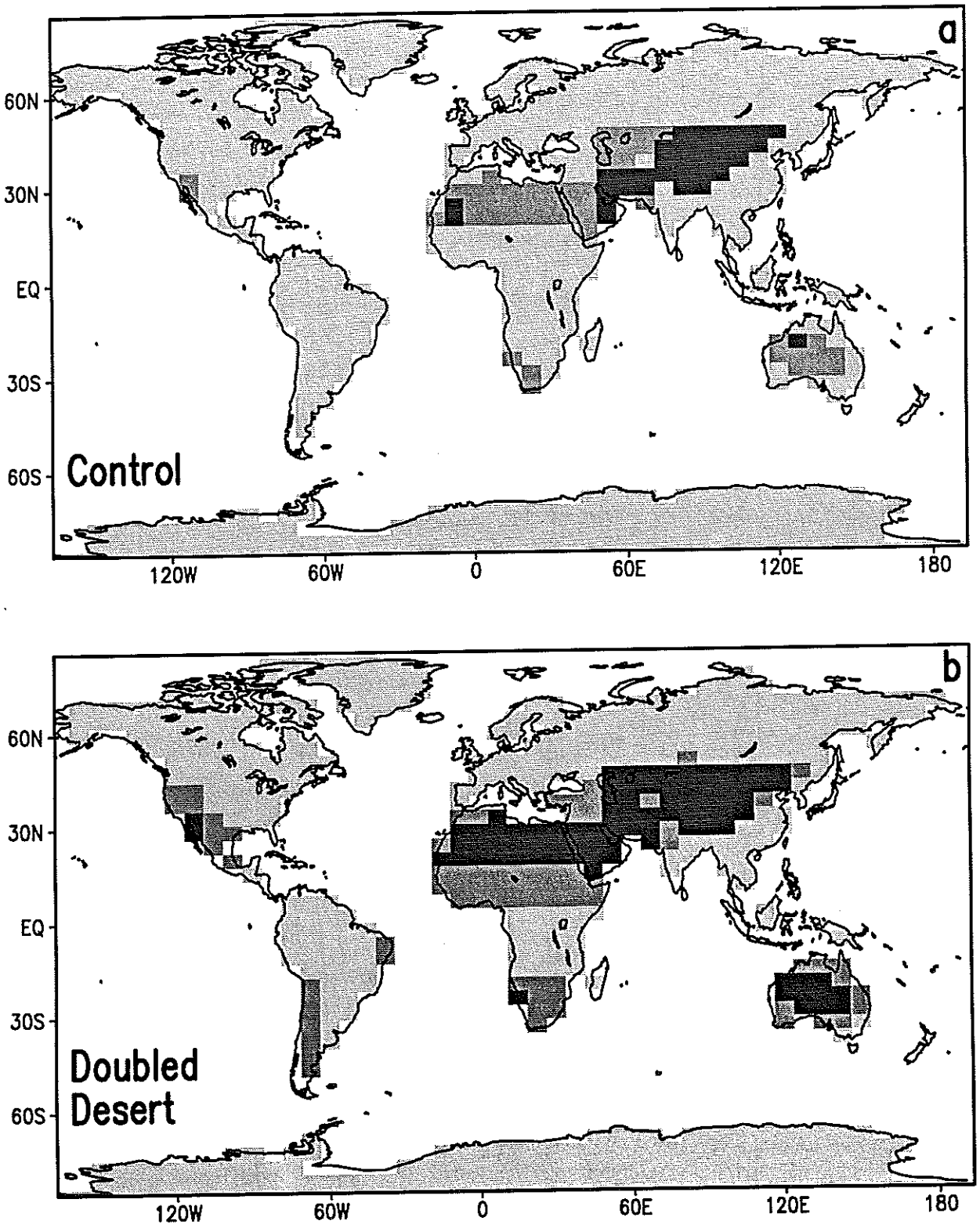
a
60N
30N
EQ
30S
60S
Control
120W
60W
0
60E
120E
180
b
60N
30N
EQ
30S
60S
Doubled
Desert
120W
60W
0
60E
120E
180
Bare Soil
Shrubs + Bare Soil
Other Land

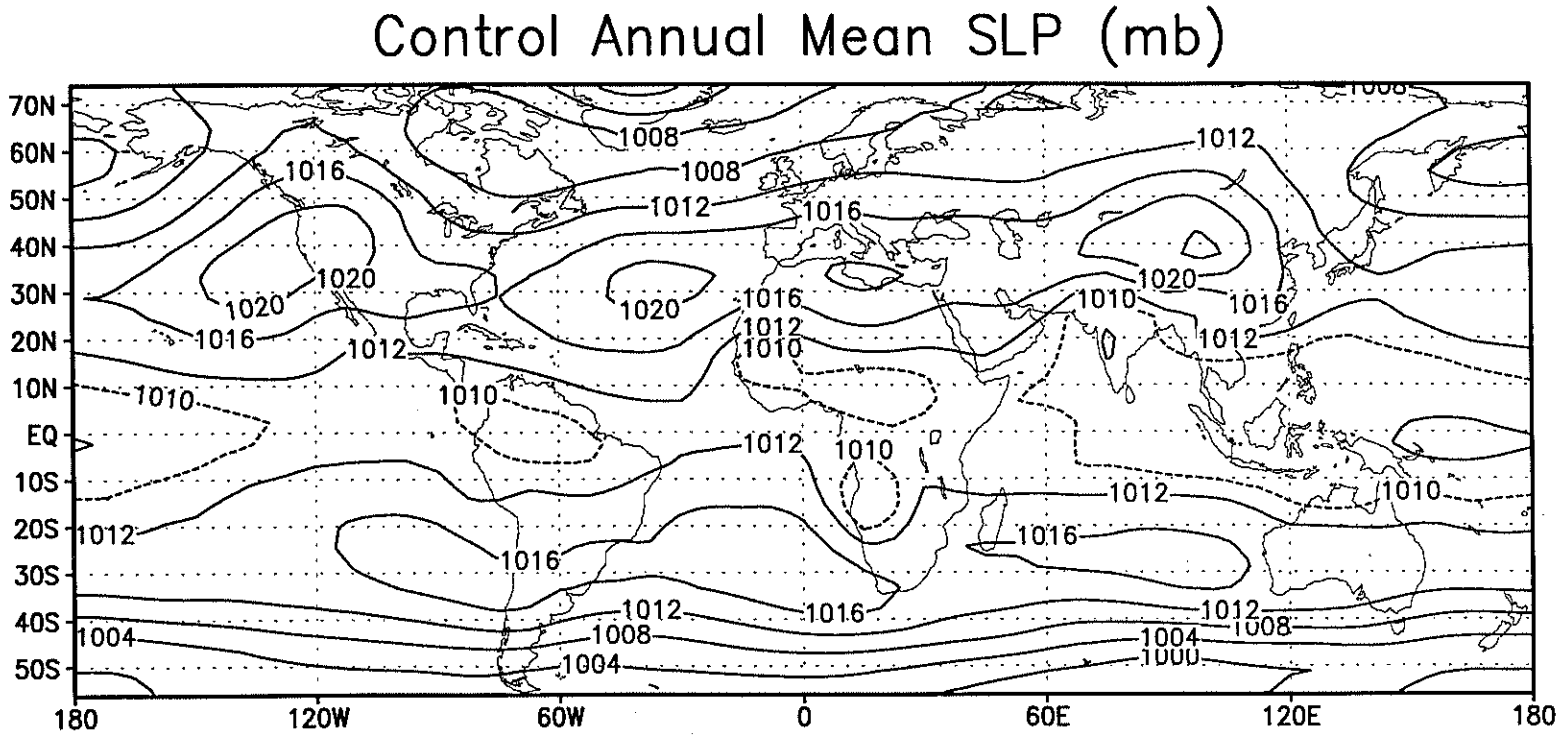
Control Annual Mean SLP (mb)
70N
60N
50N
40N
30N
20N
10N
EQ
10S
20S
30S
40S
50S
180
120W
60W
0
60E
120E
180
1008
1012
1016
1008
1012
1016
1020
1020
1020
1016
1010
1016
1012
1016
1012
1012
1010
1010
1010
1012
1010
1012
1010
1012
1016
1016
1012
1016
1012
1004
1008
1004
1004
1008
1000

Figure 2a

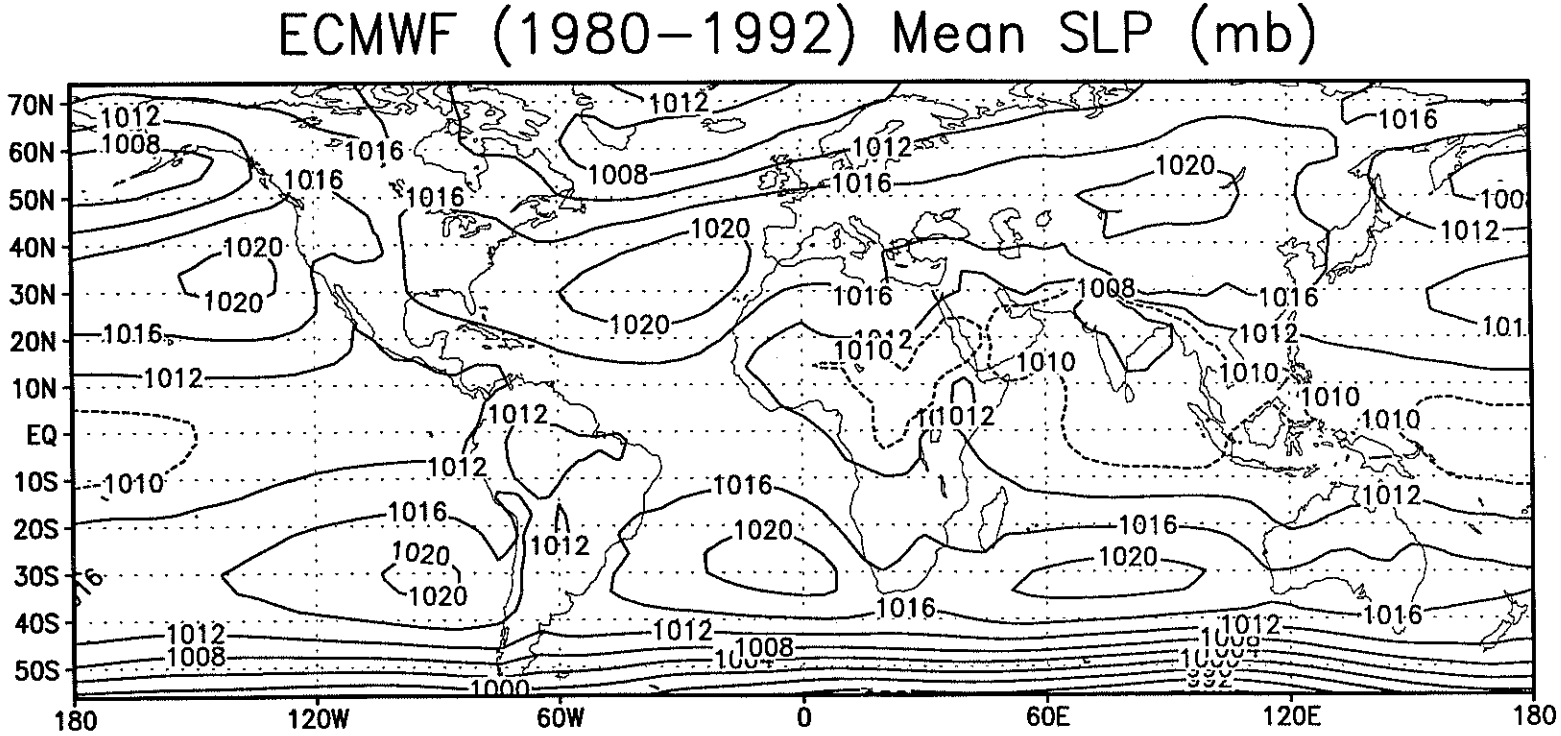
ECMWF (1980–1992) Mean SLP (mb)
70N
60N
50N
40N
30N
20N
10N
EQ
10S
20S
30S
40S
50S
180
120W
60W
0
60E
120E
180

Figure 2b

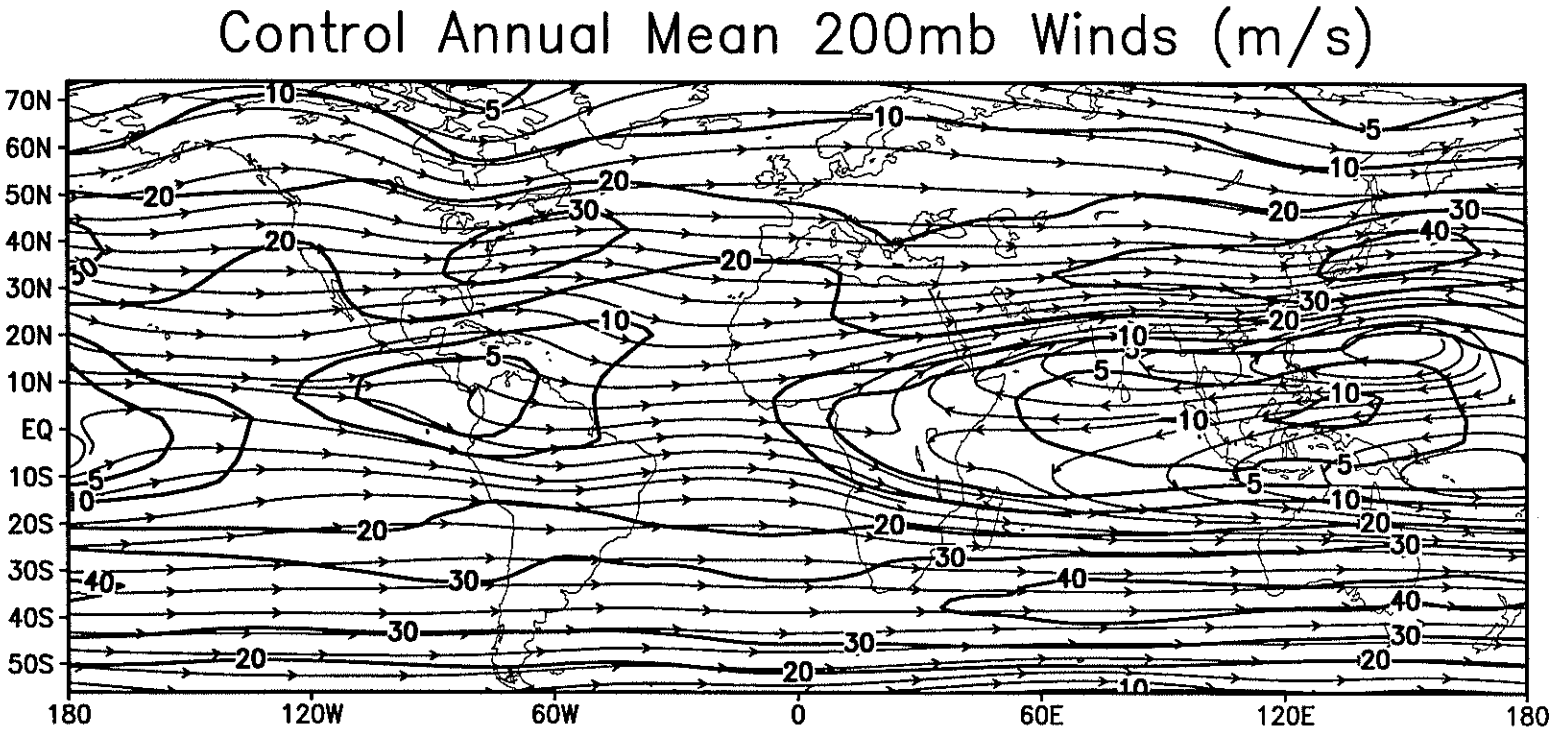
Control Annual Mean 200mb Winds (m/s)
70N
60N
50N
40N
30N
20N
10N
EQ
10S
20S
30S
40S
50S
180
120W
60W
0
60E
120E
180

Figure 3a

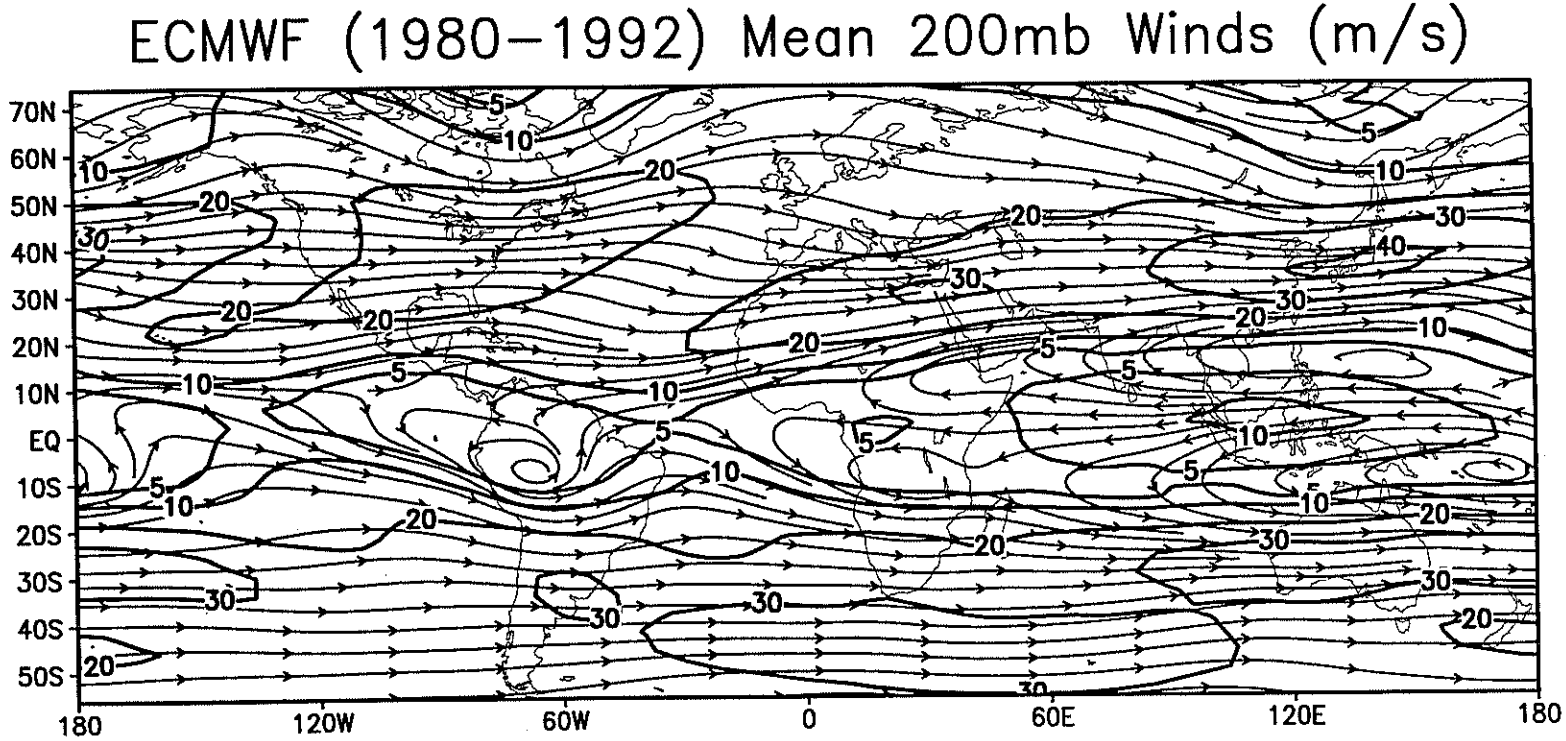
ECMWF (1980–1992) Mean 200mb Winds (m/s)
70N
60N
50N
40N
30N
20N
10N
EQ
10S
20S
30S
40S
50S
180
120W
60W
0
60E
120E
180

Figure 3b

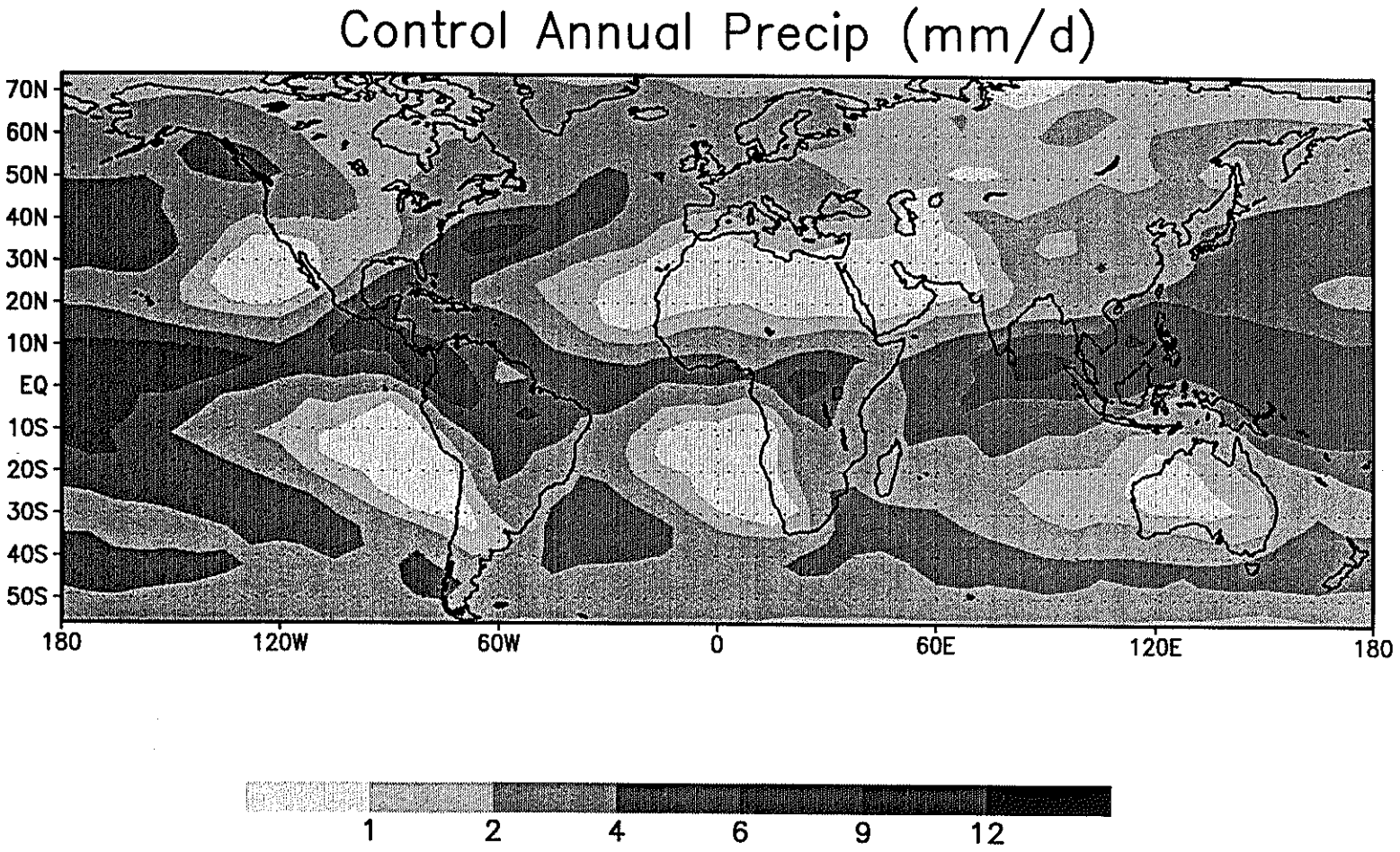
Control Annual Precip (mm/d)
70N
60N
50N
40N
30N
20N
10N
EQ
10S
20S
30S
40S
50S
180
120W
60W
0
60E
120E
180
1
2
4
6
9
12

Figure 4a

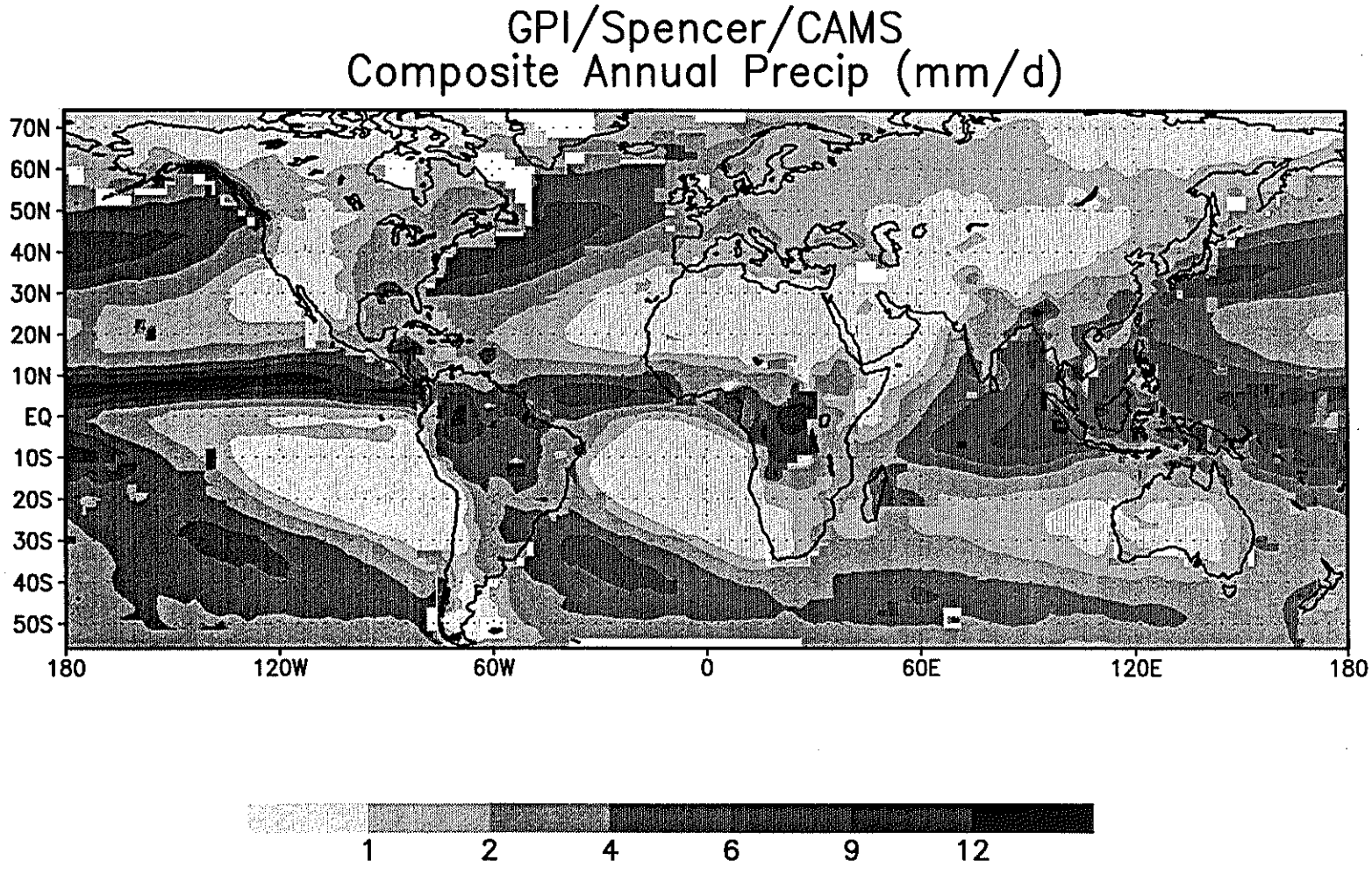
GPI/Spencer/CAMS
Composite Annual Precip (mm/d)
70N
60N
50N
40N
30N
20N
10N
EQ
10S
20S
30S
40S
50S
180
120W
60W
0
60E
120E
180
1
2
4
6
9
12

Figure 4b

Figure 5

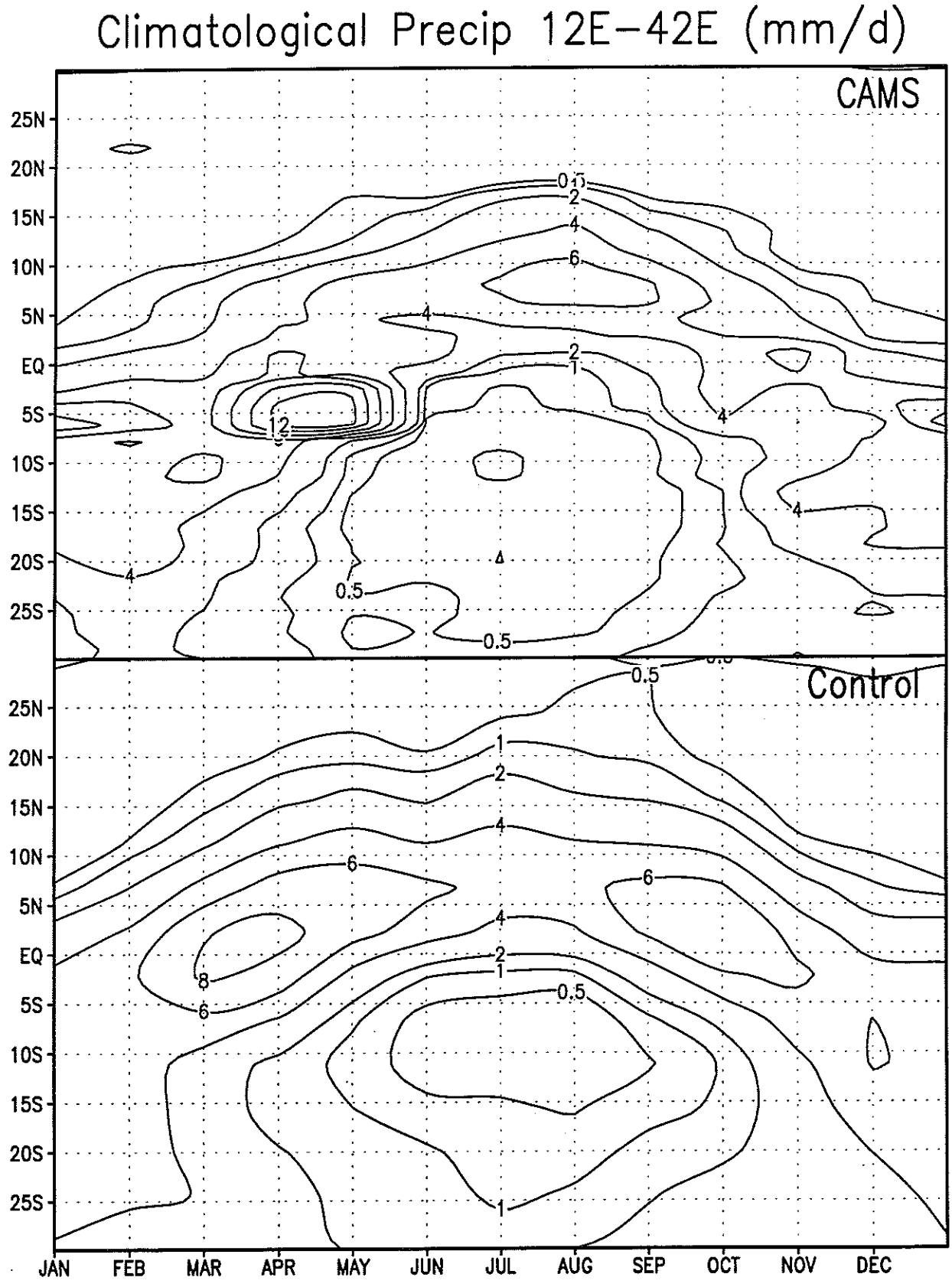
Climatological Precip 12E–42E (mm/d)
CAMS
Control
25N
20N
15N
10N
5N
EQ
5S
10S
15S
20S
25S
JAN
FEB
MAR
APR
MAY
JUN
JUL
AUG
SEP
OCT
NOV
DEC

**Figure 6**

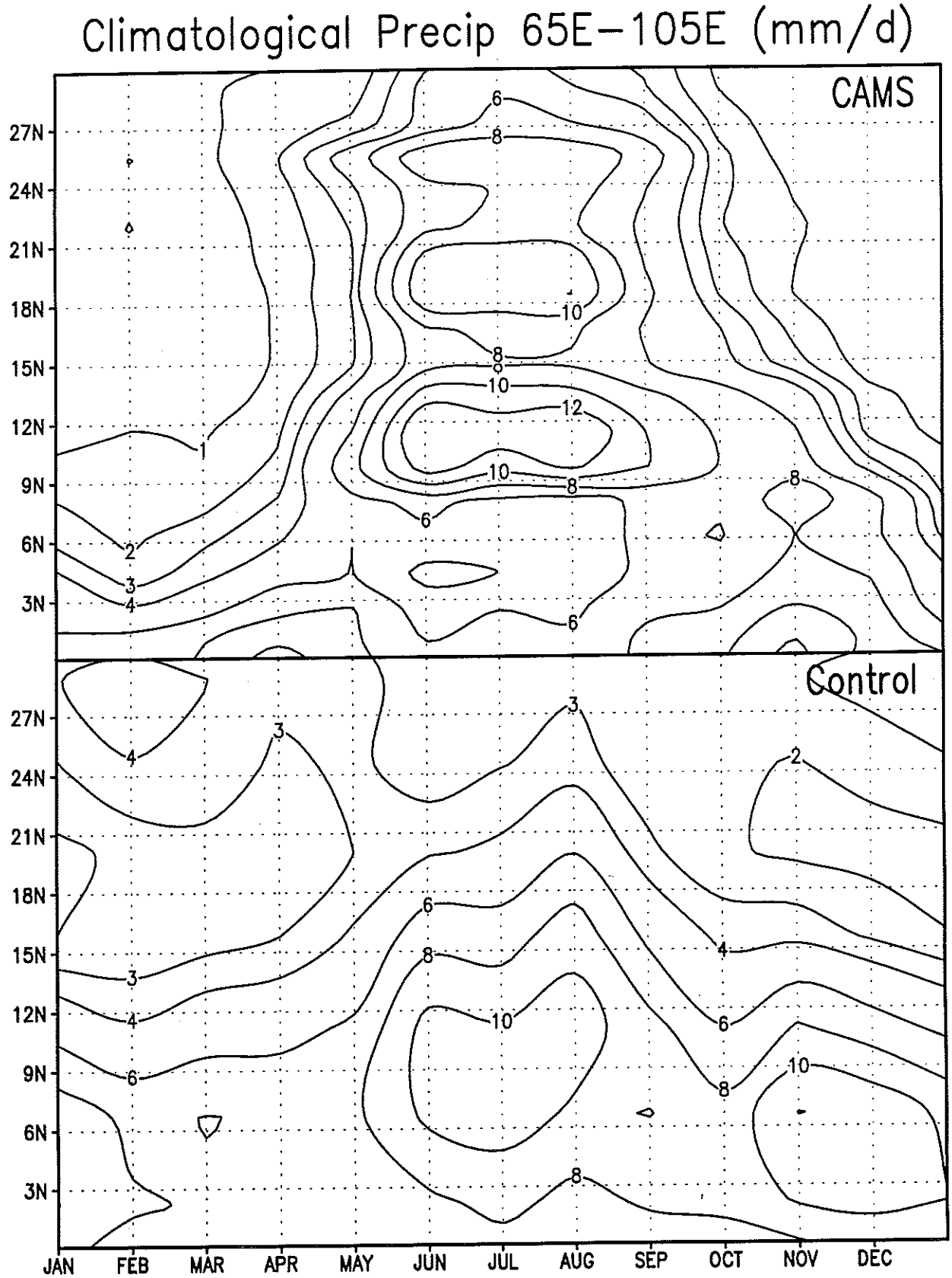
Climatological Precip 65E–105E (mm/d)
CAMS
Control
27N
24N
21N
18N
15N
12N
9N
6N
3N
JAN
FEB
MAR
APR
MAY
JUN
JUL
AUG
SEP
OCT
NOV
DEC

# 8 year Anomalies in 850–200mb Thickness (m)

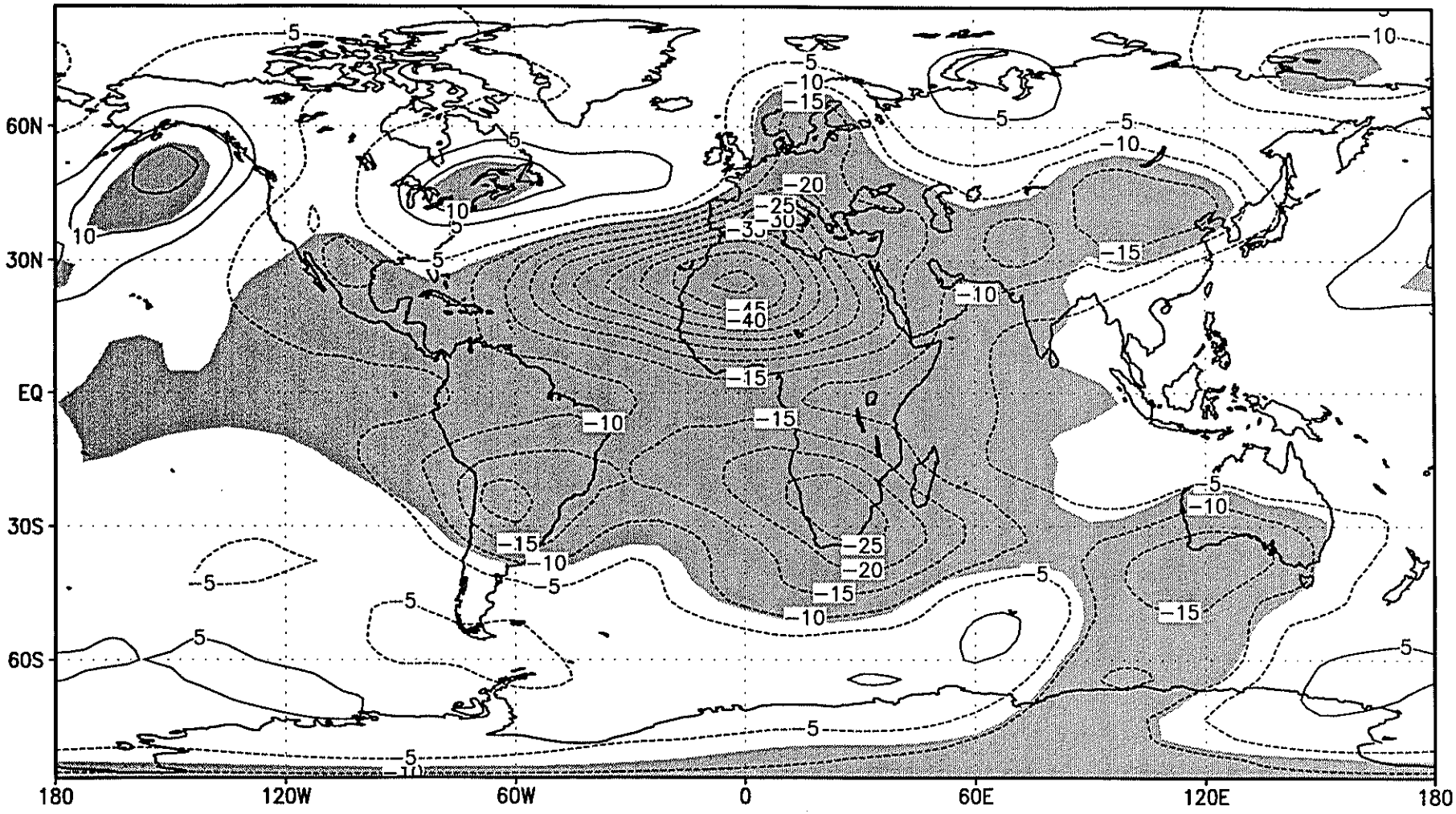


5% Significance Level

Figure 7a

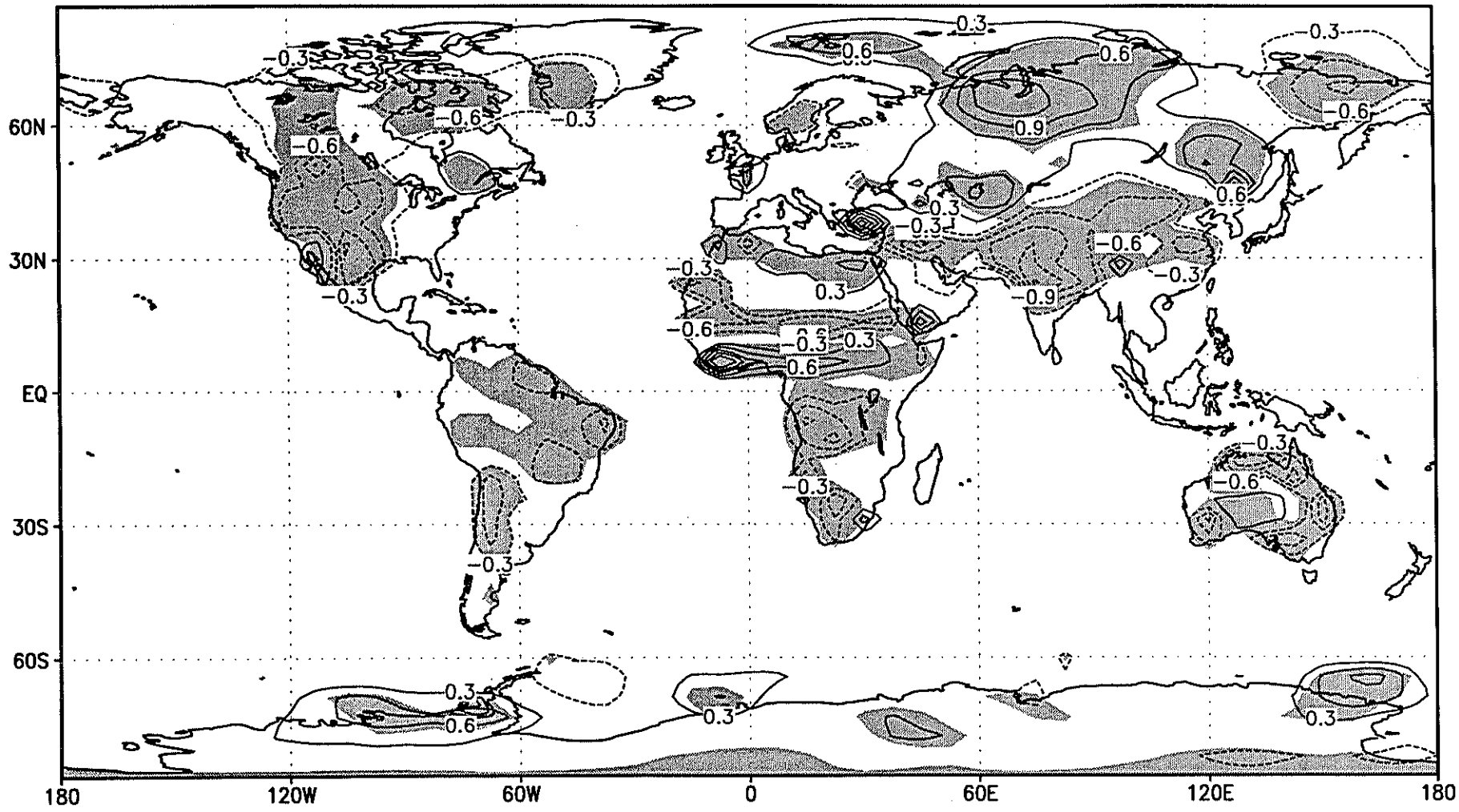
8 year Anomalies in Ts (mm/d)
60N
30N
EQ
30S
60S
180
120W
60W
0
60E
120E
180
5% Significance Level

Figure 7b

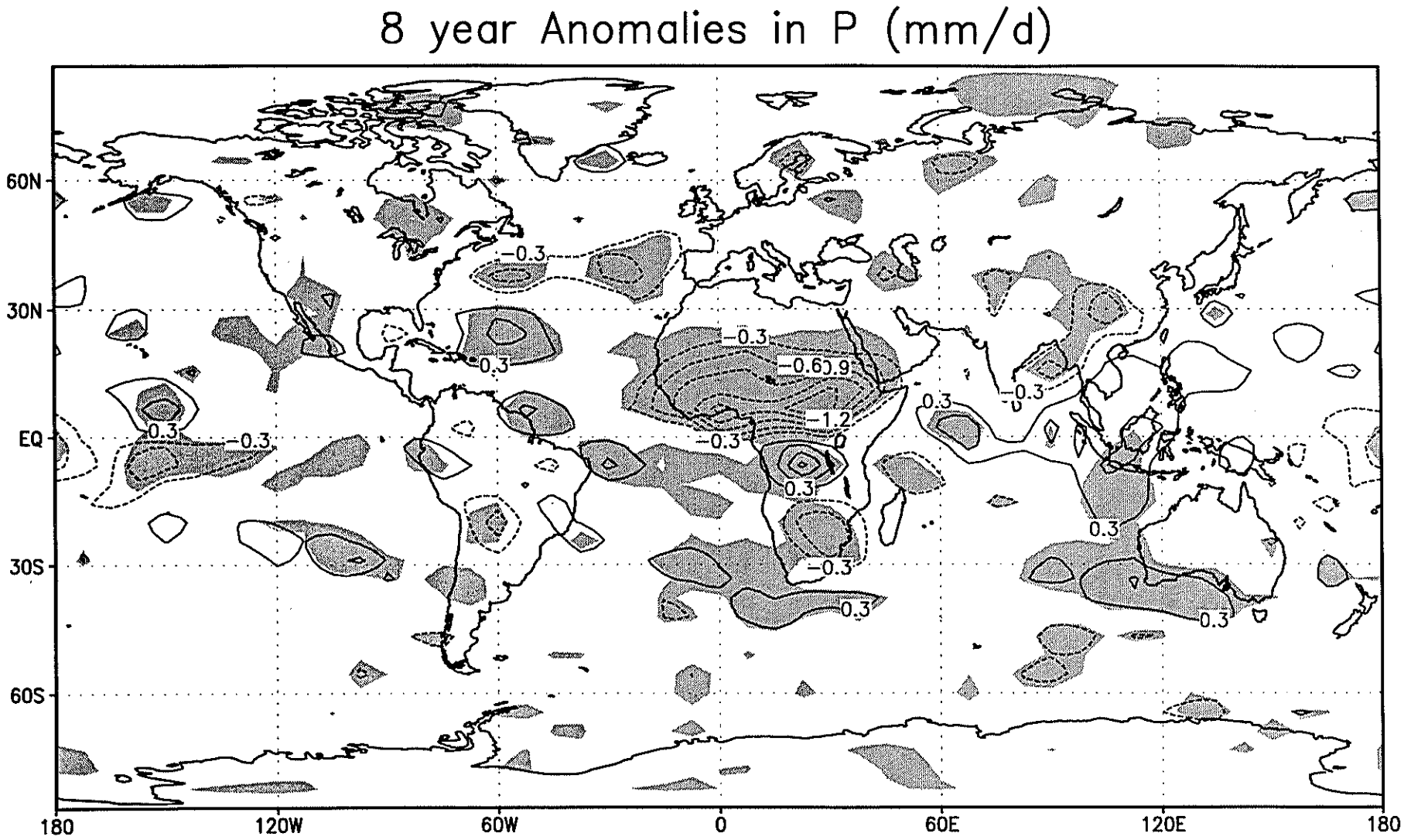
8 year Anomalies in P (mm/d)
60N
30N
EQ
30S
60S
180
120W
60W
0
60E
120E
180
-0.3
-0.3
-0.3
-0.6
0.9
-1.2
0
-0.3
0.3
-0.3
0.3
0.3
0.3
-0.3
0.3
0.3
0.3
-0.3
0.3
5% Significance Level

Figure 8a

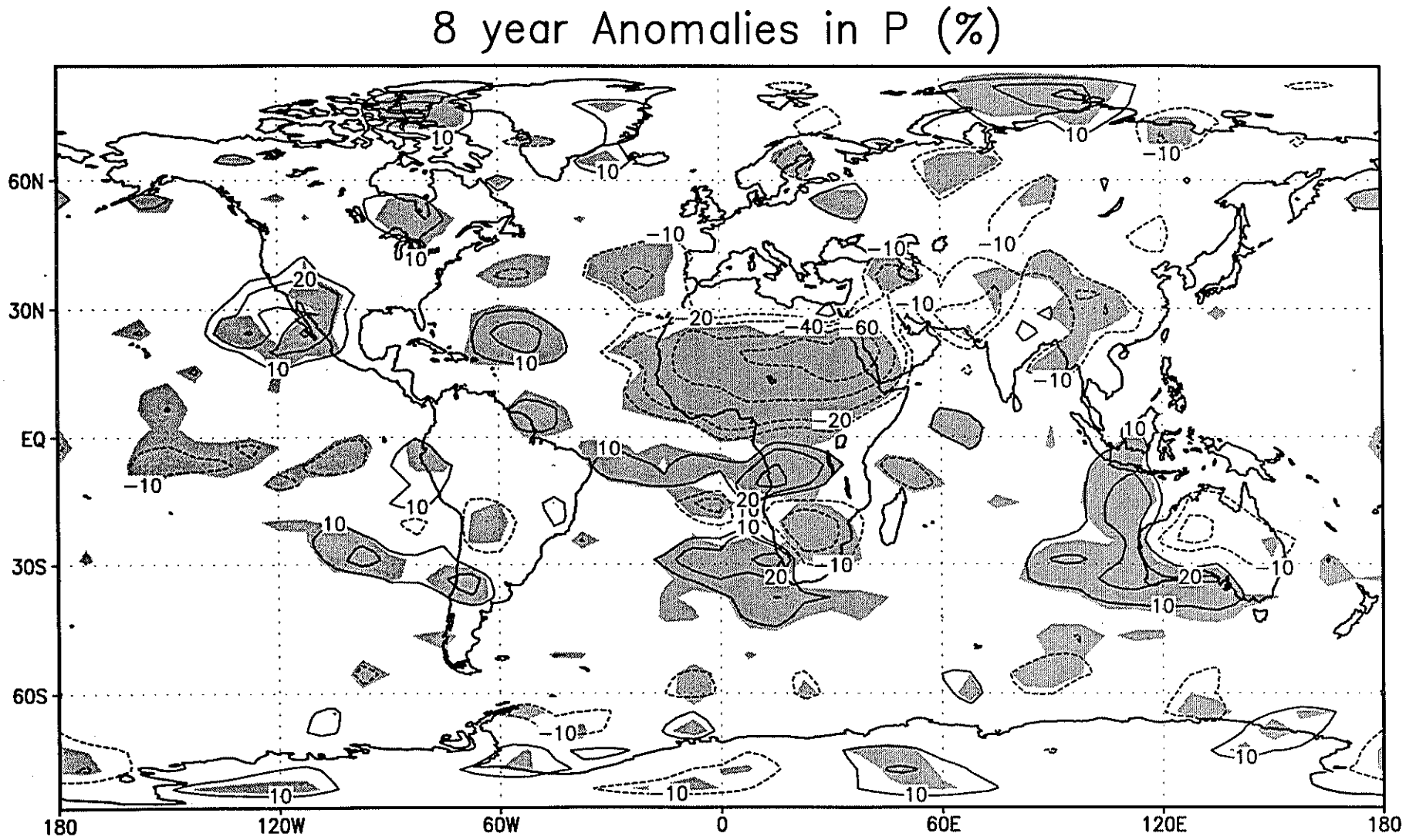
8 year Anomalies in P (%)
60N
30N
EQ
30S
60S
180
120W
60W
0
60E
120E
180
5% Significance Level

Figure 8b

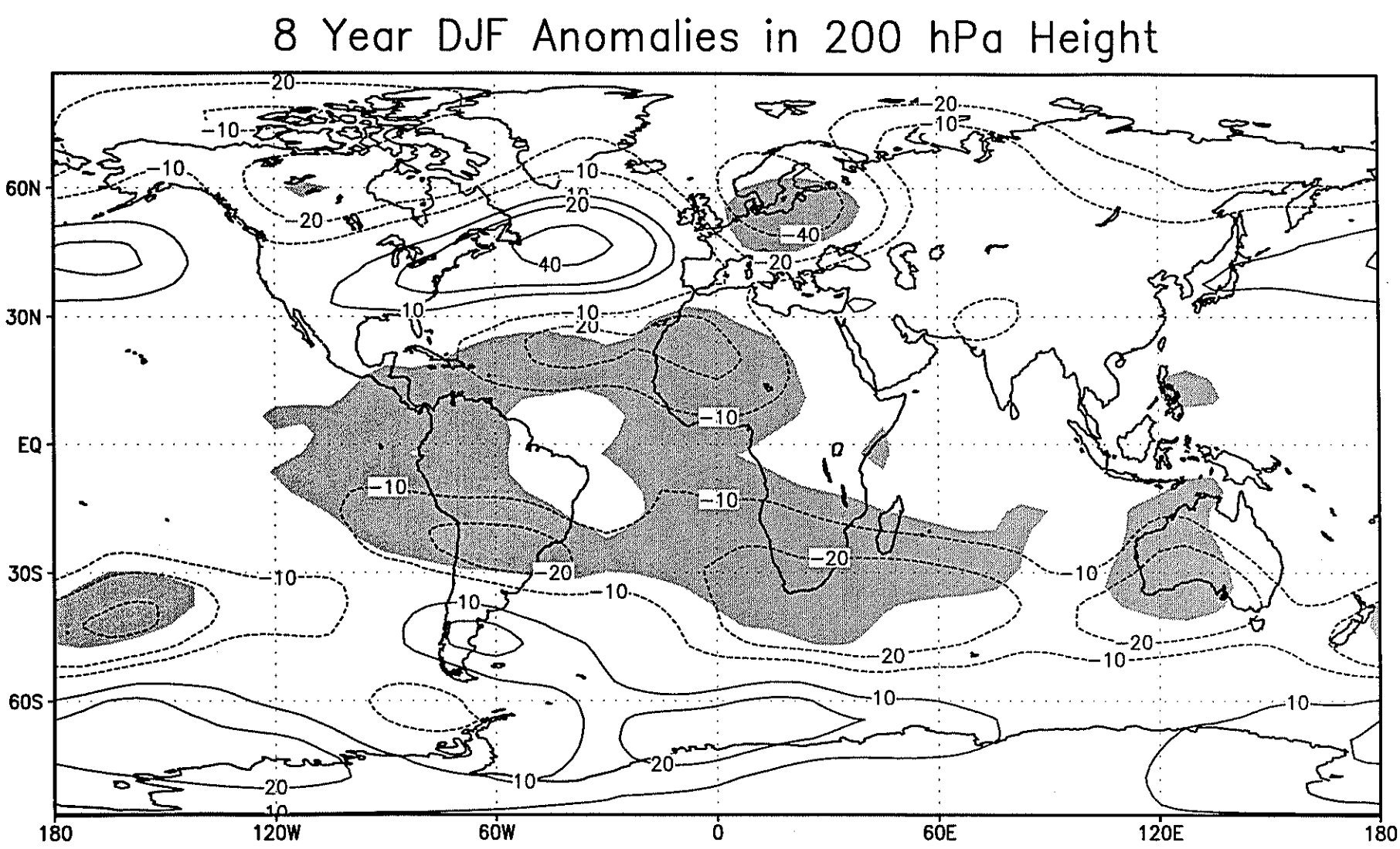
8 Year DJF Anomalies in 200 hPa Height
60N
30N
EQ
30S
60S
180
120W
60W
0
60E
120E
180
5% Significance Level

Figure 9a

# 8 Year JJA Anomalies in 200 hPa Height

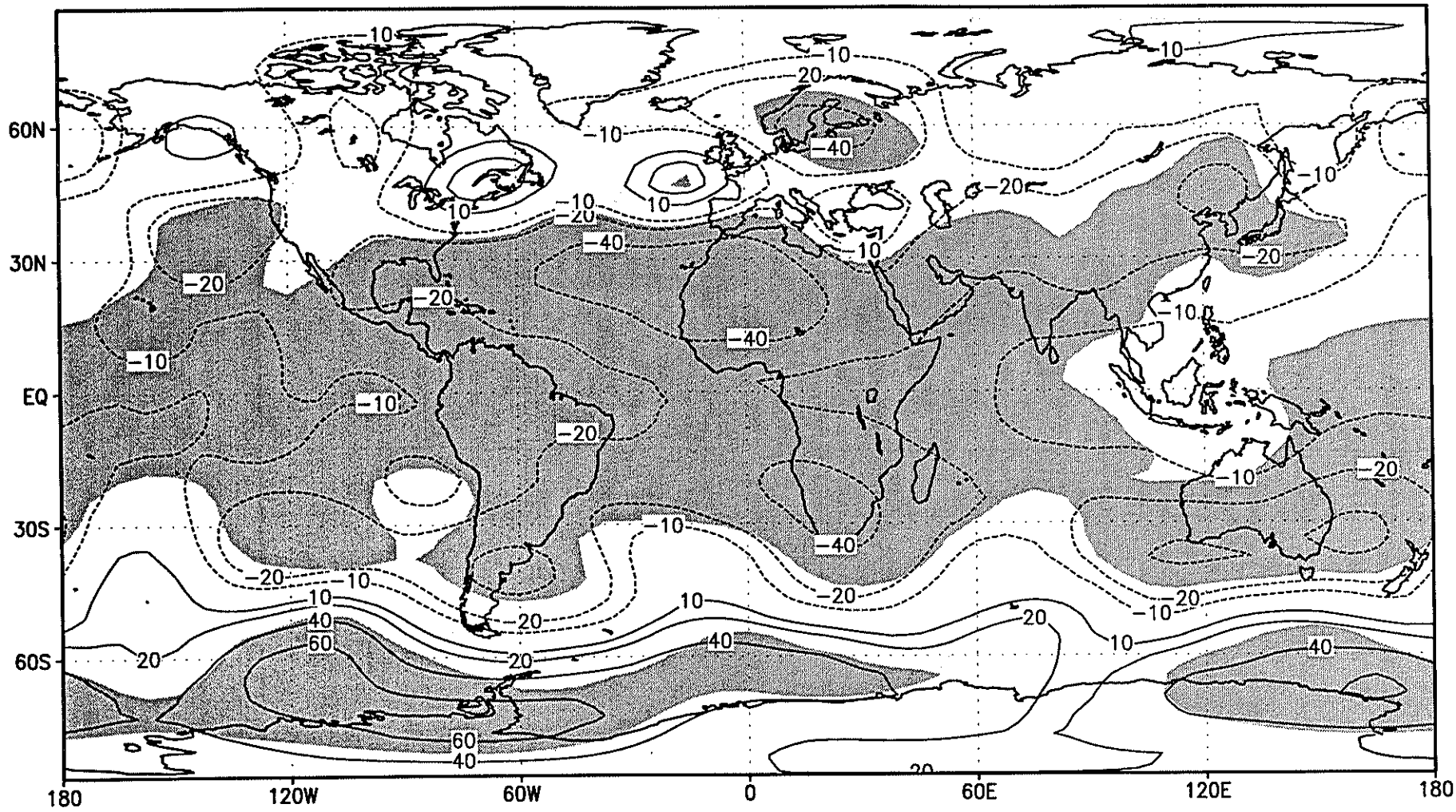


Figure 9b

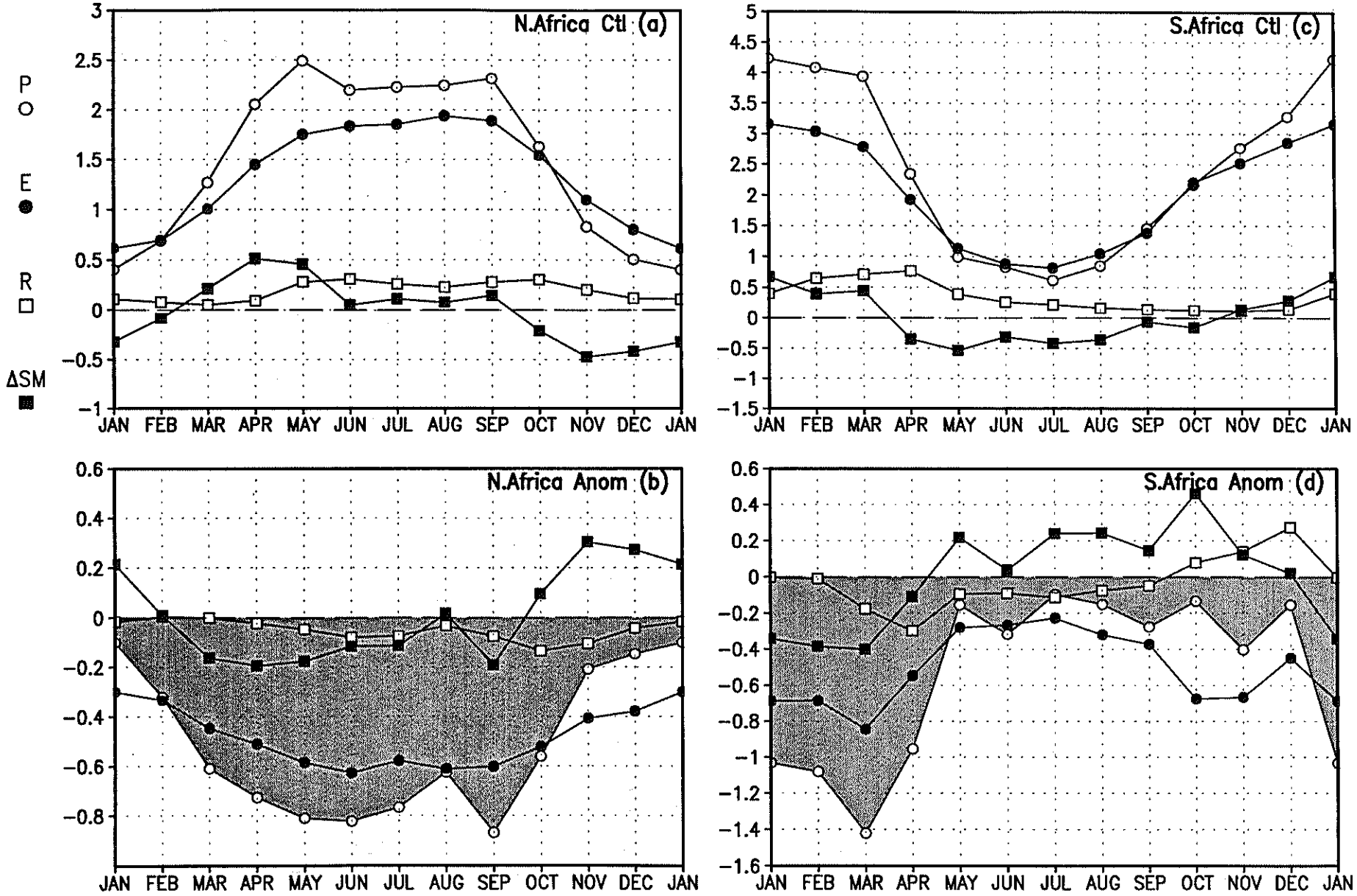
N.Africa Ctl (a)
S.Africa Ctl (c)
N.Africa Anom (b)
S.Africa Anom (d)
P
E
R
ΔSM
JAN FEB MAR APR MAY JUN JUL AUG SEP OCT NOV DEC JAN

Figure 10

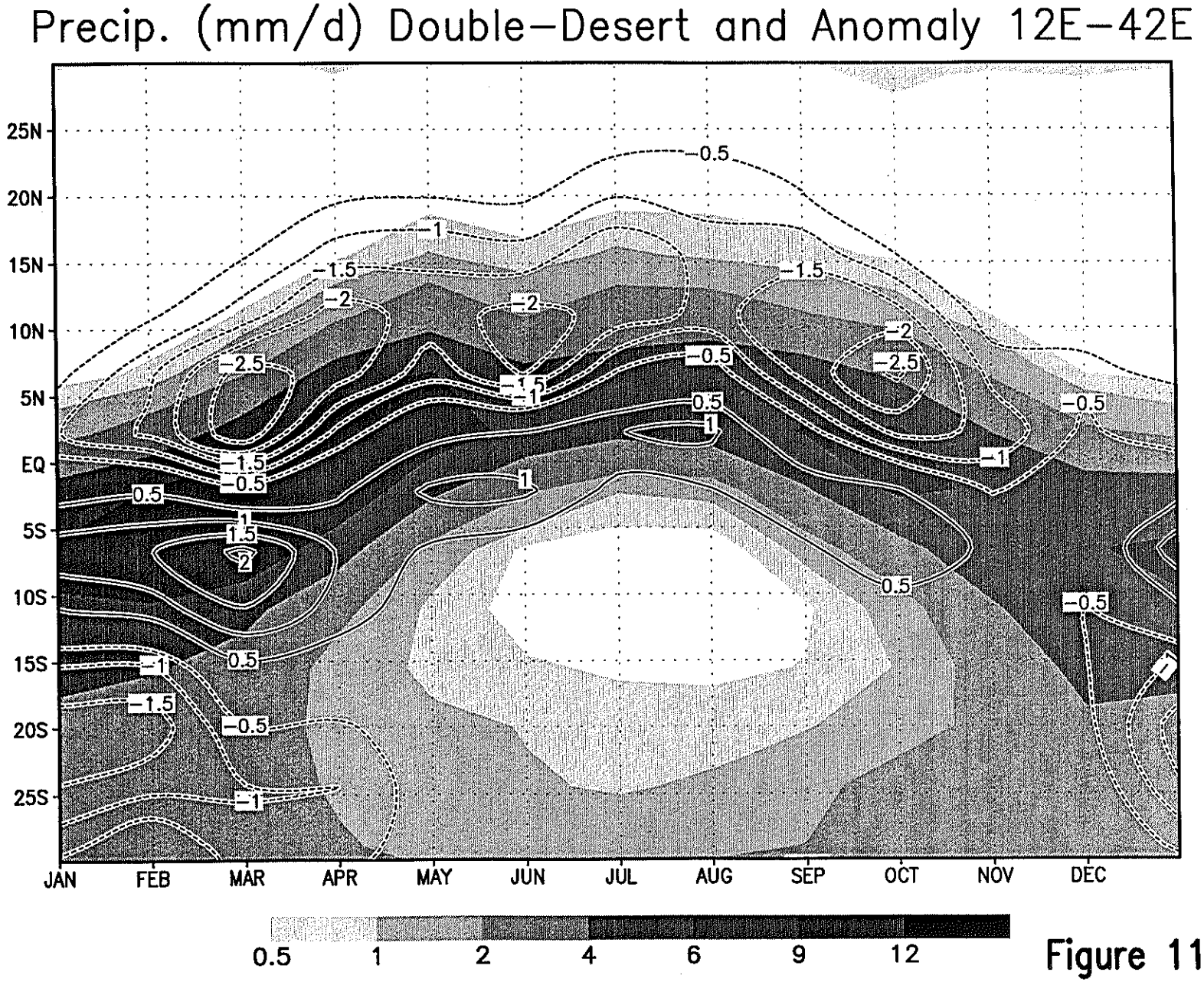
Precip. (mm/d) Double–Desert and Anomaly 12E–42E
25N
20N
15N
10N
5N
EQ
5S
10S
15S
20S
25S
JAN
FEB
MAR
APR
MAY
JUN
JUL
AUG
SEP
OCT
NOV
DEC
0.5
1
2
4
6
9
12

Figure 11

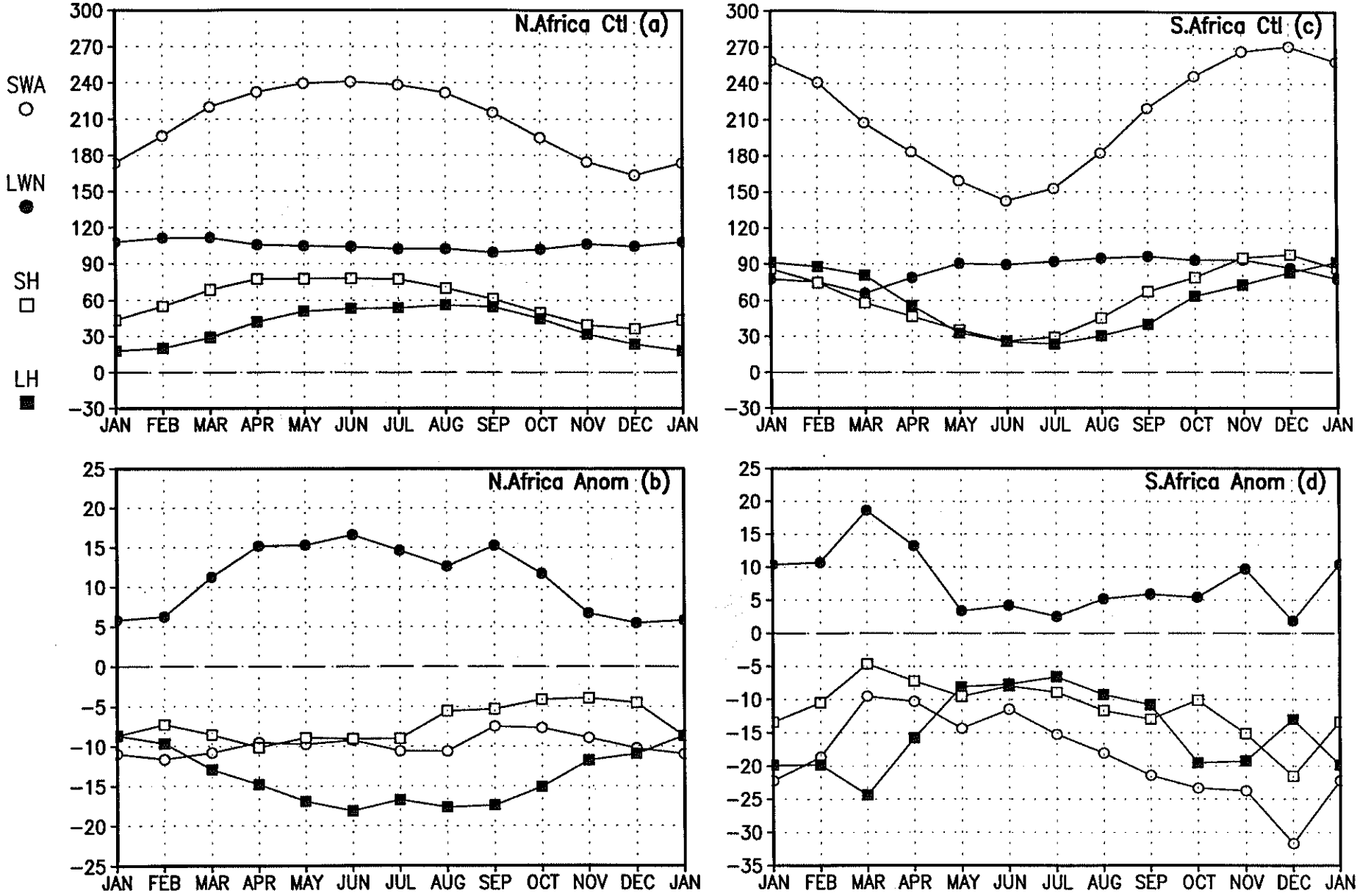
N.Africa Ctl (a)
S.Africa Ctl (c)
N.Africa Anom (b)
S.Africa Anom (d)
SWA
LWN
SH
LH
300
270
240
210
180
150
120
90
60
30
0
−30
25
20
15
10
5
−5
−10
−15
−20
−25
−35
JAN FEB MAR APR MAY JUN JUL AUG SEP OCT NOV DEC JAN

Figure 12

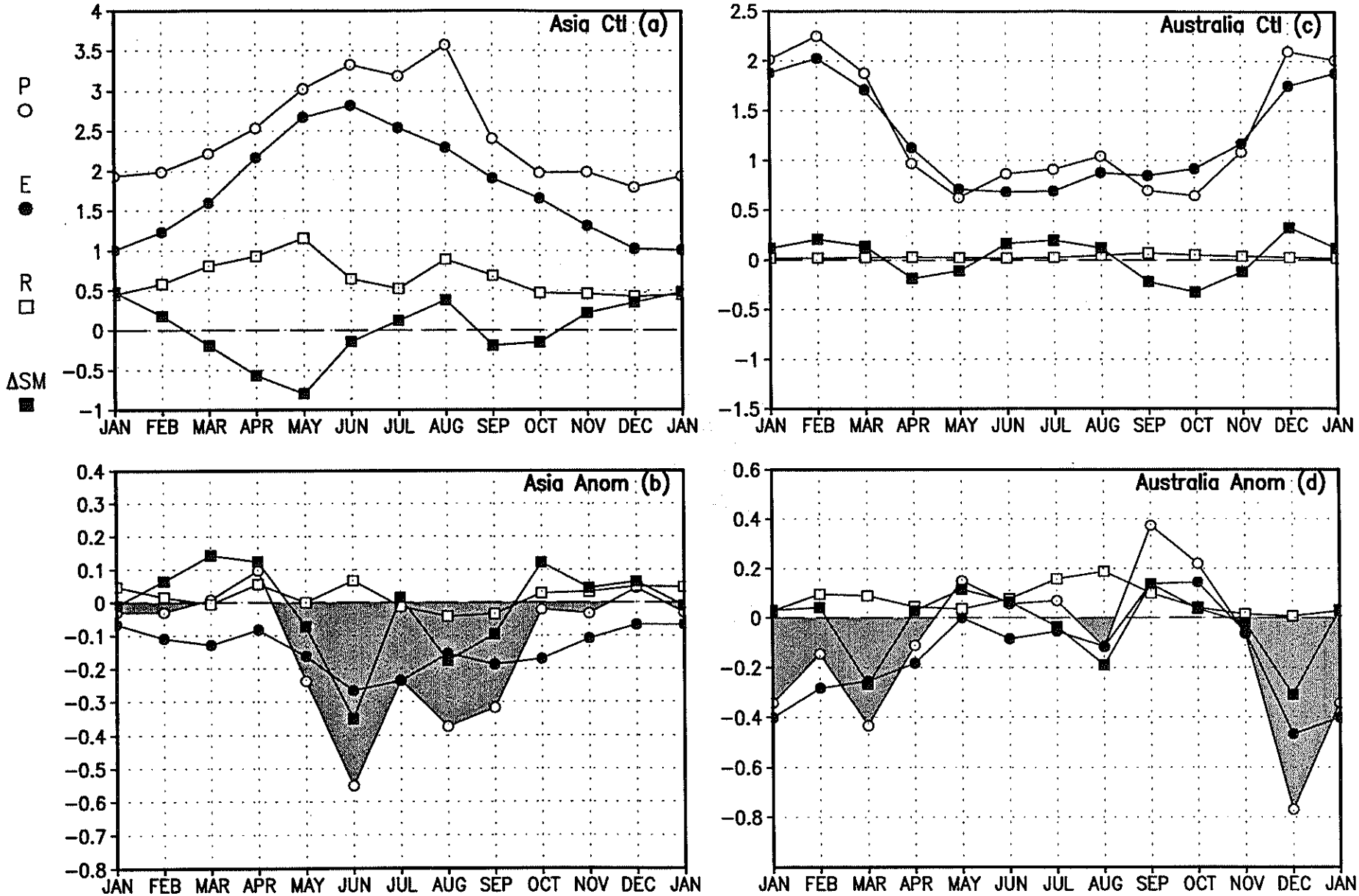
Asia Ctl (a)
Australia Ctl (c)
Asia Anom (b)
Australia Anom (d)
P
O
E
R
ΔSM
JAN FEB MAR APR MAY JUN JUL AUG SEP OCT NOV DEC JAN

Figure 13

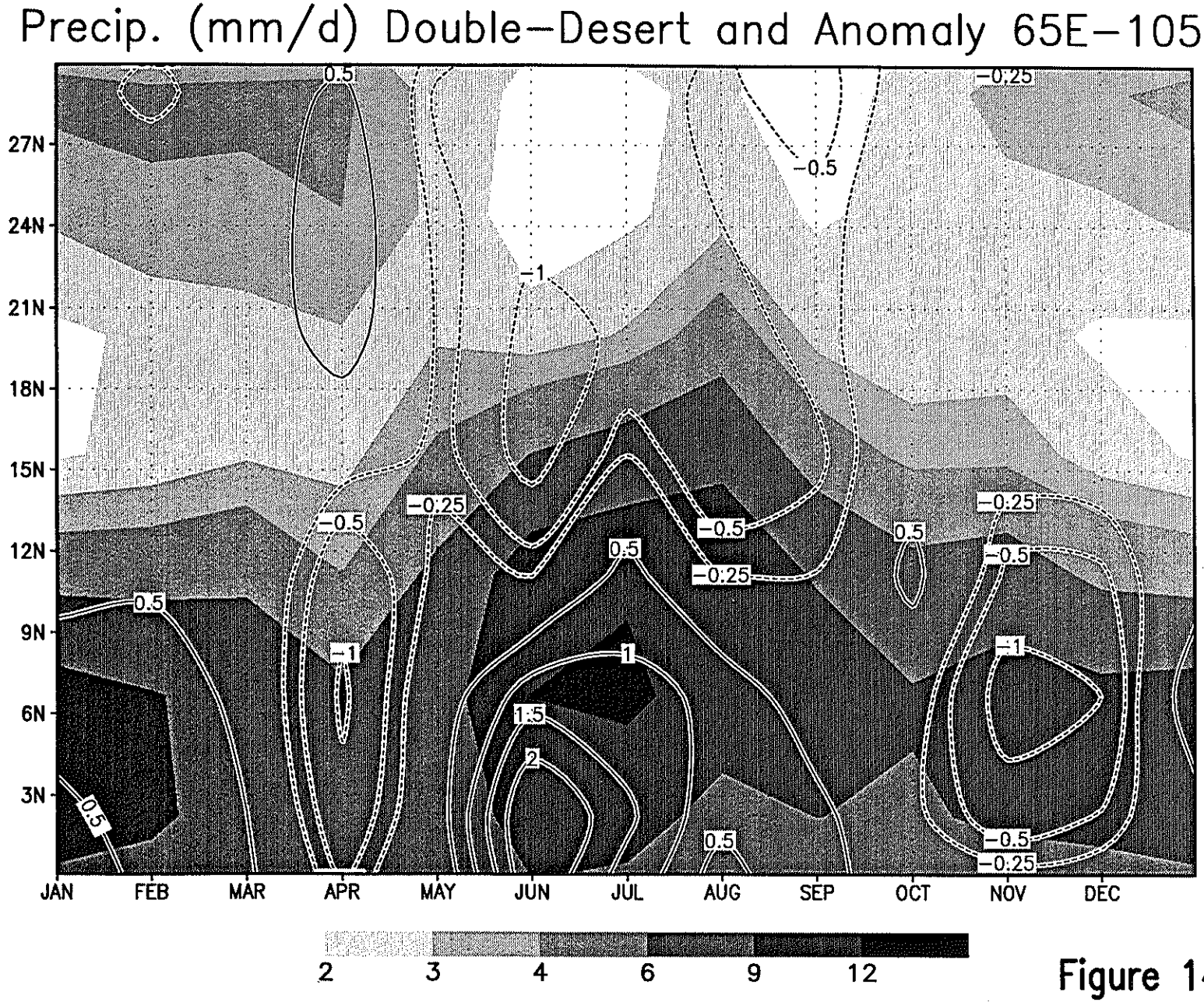
Precip. (mm/d) Double-Desert and Anomaly 65E-105E
27N
24N
21N
18N
15N
12N
9N
6N
3N
JAN
FEB
MAR
APR
MAY
JUN
JUL
AUG
SEP
OCT
NOV
DEC
0.5
-0.25
-0.5
-1
1
1.5
2
2
3
4
6
9
12

Figure 14

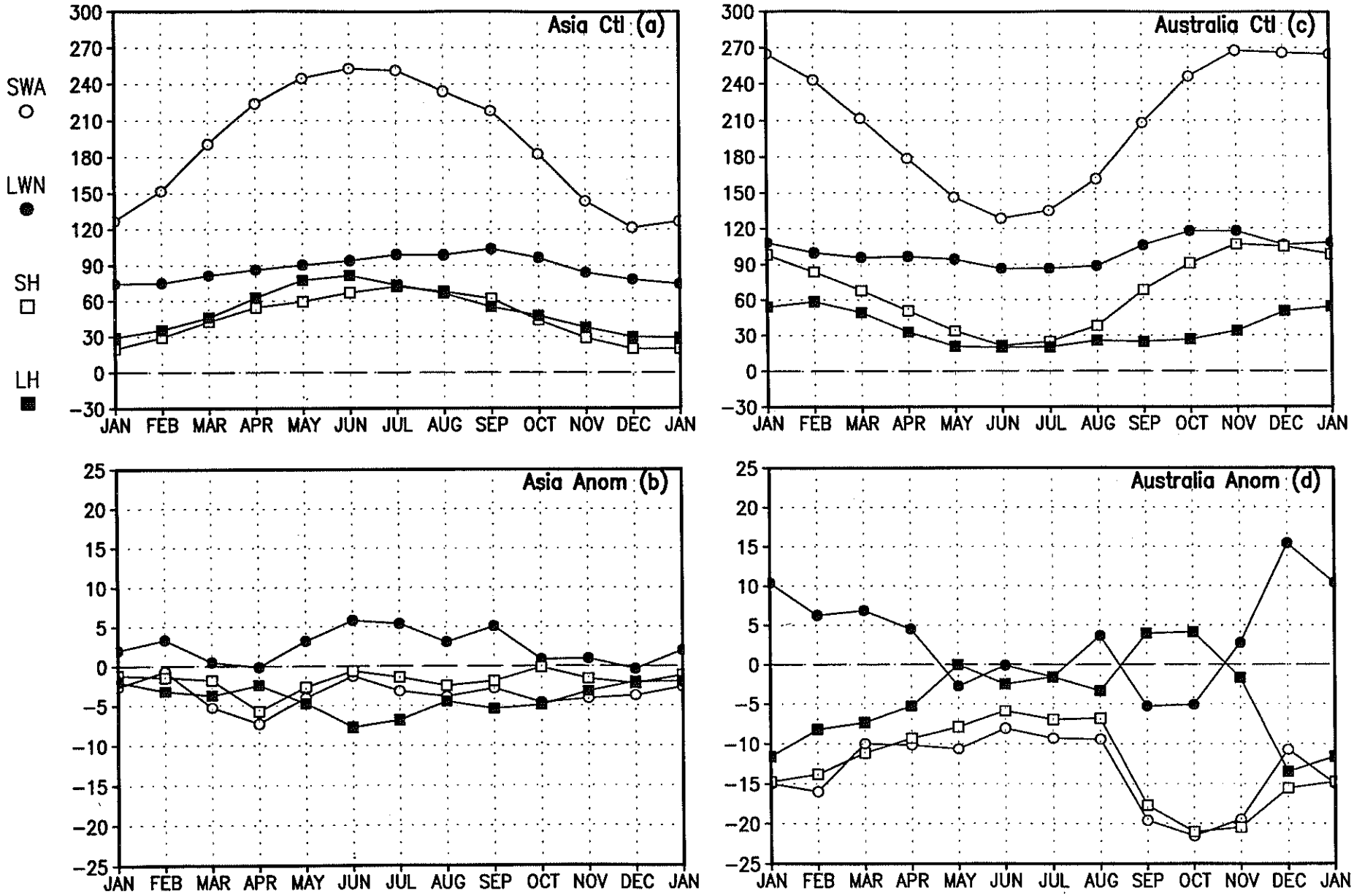
SWA
LWN
SH
LH
Asia Ctl (a)
Australia Ctl (c)
Asia Anom (b)
Australia Anom (d)
300
270
240
210
180
150
120
90
60
30
0
-30
25
20
15
10
5
-5
-10
-15
-20
-25
JAN FEB MAR APR MAY JUN JUL AUG SEP OCT NOV DEC JAN

Figure 15

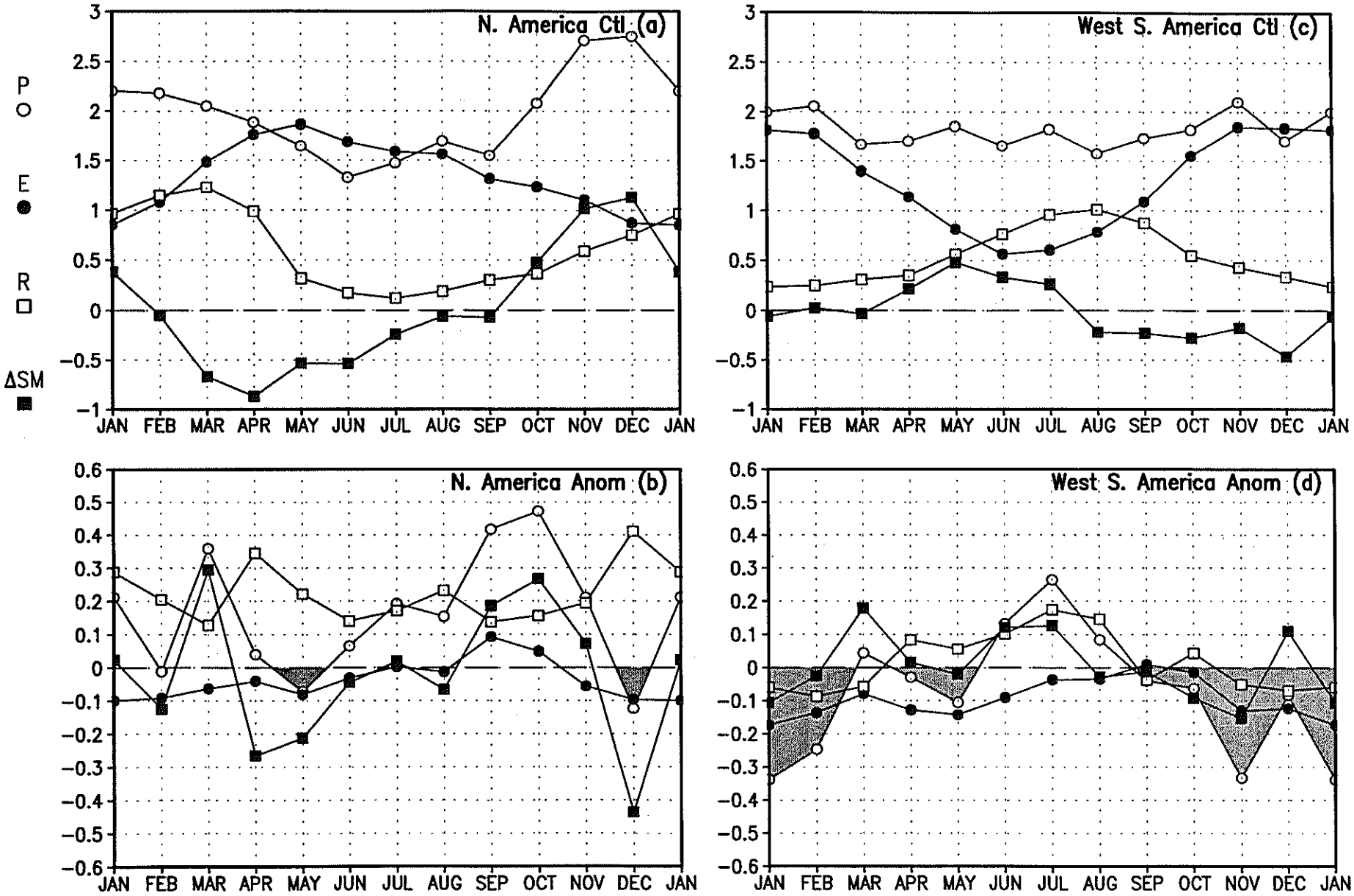
N. America Ctl (a)
West S. America Ctl (c)
N. America Anom (b)
West S. America Anom (d)
P
E
R
ΔSM
JAN FEB MAR APR MAY JUN JUL AUG SEP OCT NOV DEC JAN

Figure 16

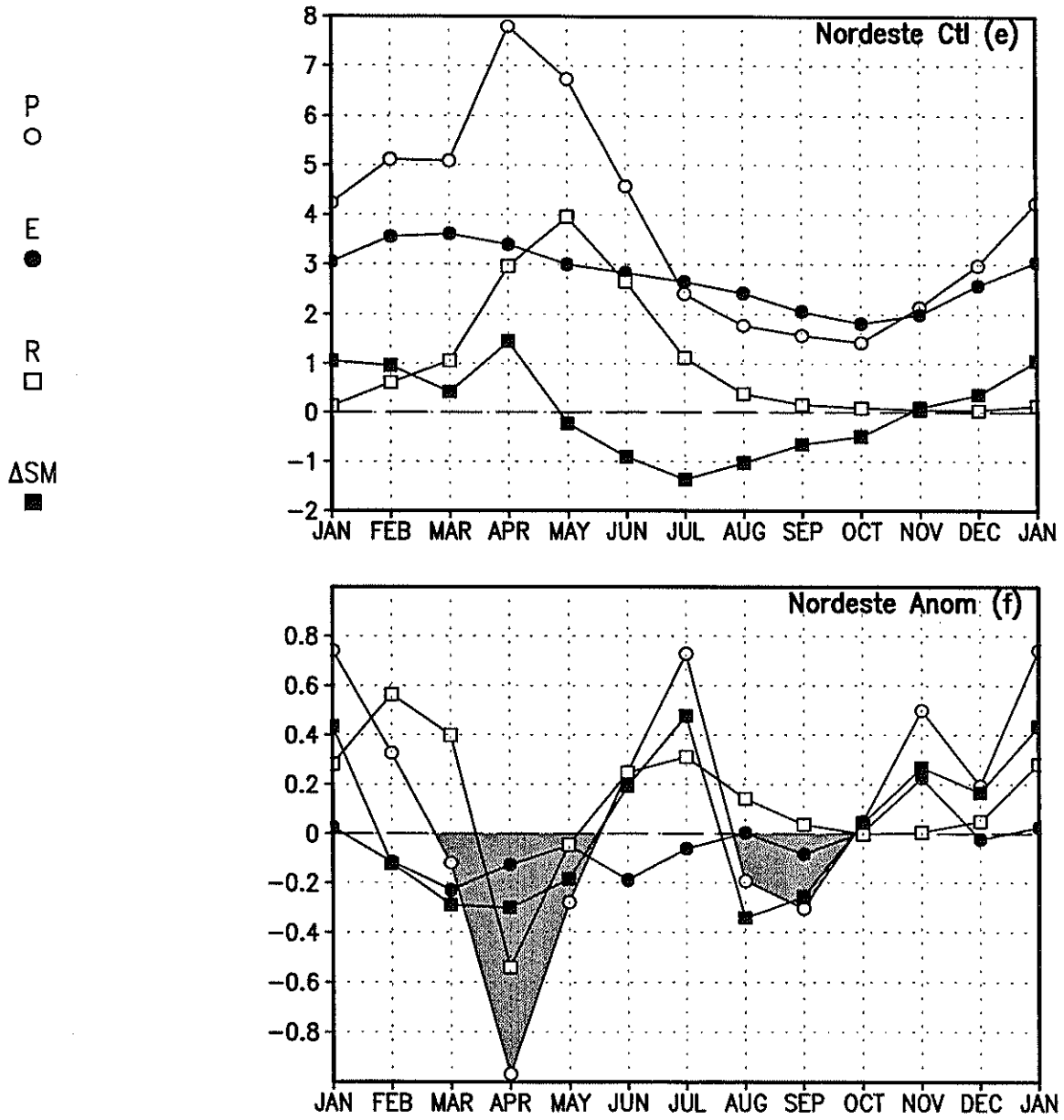


Figure 16 (cont.)